ANDRÉ GUILHERME DAUBERMANN DOS REIS

ESTABLISHMENT OF A ^{13}C-POSITIONAL ISOTOPE LABELLING APPROACH AND COMPARATIVE INVESTIGATION OF METABOLIC FLUXES IN MESOPHYLL AND GUARD CELLS

LAVRAS – MG

2020

ANDRÉ GUILHERME DAUBERMANN DOS REIS

ESTABLISHMENT OF A ^{13}C-POSITIONAL ISOTOPE LABELLING APPROACH AND COMPARATIVE INVESTIGATION OF METABOLIC FLUXES IN MESOPHYLL AND GUARD CELLS

Dissertação apresentada à Universidade Federal de Lavras, como parte das exigências do Programa de Pós-Graduação em Agronomia/Fisiologia Vegetal para obtenção do título de mestre.

Profa. Dra. Letícia dos Anjos Silva

Orientadora

Prof. Dr. Danilo de Menezes Daloso

Coorientador

LAVRAS – MG

2020

Ficha catalográfica elaborada pelo Sistema de Geração de Ficha Catalográfica da Biblioteca Universitária da UFLA, com dados informados pelo(a) próprio(a) autor(a).

Reis, André Guilherme Daubermann.
Establishment of a ^{13}C-positional isotope labelling approach and comparative investigation of metabolic fluxes in mesophyll and guard cells / André Guilherme Daubermann dos Reis. - 2020.
76 p.

Orientador(a): Letícia dos Anjos Silva.
Coorientador(a): Danilo de Menezes Daloso.
Dissertação (mestrado acadêmico) - Universidade Federal de Lavras, 2020.
Bibliografia.

1. Guard cells. 2. Tricarboxylic acid cycle. 3. ^{13}C-positional isotope labelling. I. dos Anjos, Letícia. II. Daloso, Danilo M. III. Título.

ANDRÉ GUILHERME DAUBERMANN DOS REIS

ESTABELECIMENTO DE ABORDAGEM POSICIONAL ISOTÓPICA DE ^{13}C E INVESTIGAÇÃO COMPARATIVA DE FLUXOS METABÓLICOS EM CÉLULAS MESOFÍLICAS E CÉLULAS-GUARDA

ESTABLISHMENT OF A ^{13}C-POSITIONAL ISOTOPE LABELLING APPROACH AND COMPARATIVE INVESTIGATION OF METABOLIC FLUXES IN MESOPHYLL AND GUARD CELLS

Dissertação apresentada à Universidade Federal de Lavras, como parte das exigências do Programa de Pós-Graduação em Agronomia/Fisiologia Vegetal para obtenção do título de mestre.

APROVADA em 10 de agosto de 2020.

Dra. Letícia dos Anjos	UFC
Dr. Danilo de Menezes Daloso	UFC
Dr. David Barbosa Medeiros	MPI-MP
Dra. Rebeca Patrícia Omena Garcia	UFV

Dra. Letícia dos Anjos

Orientadora

LAVRAS – MG

2020

Dedico este trabalho à minha família, cujo amor, carinho e educação são os alicerces que me possibilitaram chegar até aqui, e à minha companheira Marcella Chaves, cujo apoio foi fundamental durante essa jornada.

ACKNOWLEDGMENTS

I sincerely appreciate with deep gratitude the help and support provided by the following people and institutions that in one way or another have contributed to make this study possible.

Dr. Letícia dos Anjos Silva, my Advisor, whose support and advice throughout the research was essential.

Dr. Danilo Menezes Daloso, my Co-advisor, that also had an essential role in my researches.

Ms. Valéria Lima, for all the contributions made in this research.

To all Laboratory of Plant Metabolism (LABPLANT – UFC) students, for their time, cooperation, support and effort to the performance of this work.

To the authors that kindly provided their data of already published works.

Institutions:

National Council for the Improvement of Higher Education (CAPES).

National Council for Scientific and Technological Development (CNPq).

Federal University of Lavras (UFLA).

Federal University of Ceará (UFC).

“*The good life is one inspired by love and guided by knowledge. Neither love without knowledge nor knowledge without love can produce a good life*.”

Bertrand Russell

RESUMO

As células-guarda respondem à diversos estímulos que resultam na alteração do seu volume e, como consequência, na abertura ou fechamento do poro estomático. Diversos estímulos ocasionam mudanças no volume das células guarda, como por exemplo luz, CO_2 e fitohormônios. As células-guarda possuem um metabolismo com diversas particularidades, em comparação com as células mesofílicas. Por exemplo, enquanto o fluxo metabólico através do ciclo do ácido tricarboxílico (TCA) é inibido pela luz em células mesofílicas, evidências sugerem que o ciclo TCA e a glicólise de células guarda sejam ativados na presença de luz. Dentro desta perspectiva, este trabalho objetivou investigar os fluxos metabólicos através do ciclo TCA e de rotas metabólicas associadas, como da glicólise, da fixação de CO_2 mediada pela enzima fosfo*enol*piruvatocarboxilase (PEPc) e da síntese de amino ácidos como Ala, Glu e Gln. Para isso, foi estabelecido uma abordagem de marcação isotópica (^{13}C) posicional utilizando dados previamente publicados de cromatografia gasosa acoplada à espectrometria de massas. Diversos metabólitos do ciclo TCA e de rotas metabólicas associadas foram avaliados em termos de abundância relativa do isotopômero, enriquecimento total de ^{13}C e conteúdo dos metabólitos. Os resultados obtidos para células-guarda foram comparados com resultados de células mesofílicas de plantas C3 e C4, bem como com os de células mesofílicas de folhas fonte e dreno de plantas C3. Nesse sentido, os resultados sugerem que as células-guarda têm um modo particular de fluxo do ciclo TCA, e das rotas associadas, com certas similaridades com células-dreno de plantas C3. Além disso, os resultados indicam que a inibição dependente de luz da piruvato desidrogenase restringe severamente o fluxo do ciclo TCA em direção à síntese de glutamato.Os resultados são discutidos no contexto da regulação do ciclo TCA e do metabolismo de células guarda.

Palavras-chave: Ciclo do ácido tricarboxílico, fluxo metabólico, glutamina, marcação isotópica posicional, metabolismo de células guarda, regulação metabólica.

ABSTRACT

Guard cells respond to a wide range of stimuli in order to change its volume and, thus, open or close the stomatal pore. Several stimuli cause changes in guard cells turgor, such as light, CO_2, phytohormones, among others. Guard cells metabolism have differences in comparison with mesophyll cells. For instance, whilst the metabolic flux throughout the tricarboxylic acid (TCA) cycle is inhibited by light in mesophyll cells, evidences suggest that guard cells TCA cycle is active in presence of light. In this sense, this work aimed to investigate the metabolic fluxes through the TCA cycle and other associated pathways, such as glycolysis and CO_2 fixation mediated by phospho*enol*pyruvate carboxylase (PEPc). For this purpose, we stablished a mass spectrometry-based ^{13}C-positional isotope labelling approach to analyse previously published gas-chromatography coupled to mass spectrometry data. Several metabolites of, or associated to the TCA cycle were evaluated in terms of relative isotopomer abundance, total ^{13}C-enrichment and metabolite content, and the results from guard cells were compared with mesophyll cells of C3 or C4 plants, as well as to source or sink C3-mesophyll cells. In this sense, the results suggest that guard cells have a particular metabolic flux mode throughout TCA cycle and associated pathways, with certain similarities with mesophyll cells of C3 plants. Furthermore, the results indicate that the light-dependent inhibition of pyruvate dehydrogenase severely restricts the fluxes of carbon to glutamate synthesis. Results are discussed in the context of TCA cycle regulation and guard cell metabolism.

Key words: ^{13}C-positional isotope labelling, glutamine, guard cells metabolism, metabolic fluxes, metabolic regulation, tricarboxylic acid cycle.

SUMMARY

FIRST PART

1. GENERAL OVERVIEW

In plants, leaf cuticle is impermeable to water and CO_2. Thus, gas exchange in leaves mostly occurs through the stomatal pore, which regulates the balance between CO_2 uptake for photosynthesis and water loss by transpiration. Stomatal opening process is controlled by changes in the metabolism of the surrounding specialized leaf epidermal cells, named guard cells (GCs). There are several endogenous and environmental signals governing stomatal movement. For instance, stomatal opening is regulated endogenously by phytohormones, circadian rhythms (HASSIDIM et al., 2017) and other metabolites coming from mesophyll cells. In addition, stomatal movement also responds to light (SHIMAZAKI et al., 2007), plant water status (TARDIEU & SIMONNEAU, 1998), CO_2 (HEATH & RUSSELL, 1954), atmosphere vapor pressure (MC ADAM & BRODRIBB, 2015) and temperature (KOSTAKI et al., 2020). However, many open questions remain open regarding the regulation of guard cells metabolism to trigger stomatal movement in response to internal e external signals. For instance, there is still a debate about what are the exact sources of carbon for the synthesis of osmoticum, required for osmotic regulation of guard cell volume, and about the source of energy required to support stomatal movements, since guard cells are known to have low photosynthetic capacity.

It has been argued that guard cell photosynthesis cannot provide all the energy necessary to guard cells osmoregulation (OUTLAW, 1989). In accordance, evidences have shown that guard cells have a low number of chloroplasts and low content of ribulose-1,5-biphosphate carboxylase/oxygenase (RubisCO) and chlorophyll (HUMBLE & RASCHKE, 1971). In contrast, guard cells have a high number of mitochondria and higher respiration rates (WILLMER & FRICKER, 1996; ARAÚJO *et al.*, 2011), when compared to mesophyll cells, suggesting that respiration is the main source of ATP for these cells. Notwithstanding, it has been shown that in leaves the pyruvate dehydrogenase complex (PDH), a key enzyme in the regulation of the TCA cycle, is inactivated by a light-dependent phosphorylation (GEMEL & RANDALL, 1992; MCDONALD & VANLERBERGHE, 2018). In guard cells, however, a recent ^{13}C-sucrose labelling study suggested a differential regulation of both glycolysis and TCA cycle in guard cells in the light (MEDEIROS *et al.*, 2018). Nonetheless, experimental evidence supporting this idea and several pieces of the guard cell metabolism puzzle are still missing.

Here we have established a gas chromatography coupled to mass spectrometry-based (GC-MS) positional ^{13}C-positional isotope labelling approach to investigate the distribution of

the carbon fixed by PEPc over the TCA cycle and glutamate (Glu)/glutamine (Gln). After establishing this approach, we performed a meta-analysis of previously published data from ^{13}C-isotope labelling experiments carried out in guard cells of Arabidopsis and tobacco, in leaves of Arabidopsis and maize, and in sink and source leaves of Arabidopsis. Collectively, our results indicate that the fluxes from glycolysis and PEPc activity toward Gln synthesis are higher in guard cells when compared with those observed in C3 or C4 mesophyll cells, and resemble metabolic fluxes observed in sink C3-mesophyll cells. Our results suggest a differential regulation of both glycolysis and the TCA cycle in GCs and are, here, discussed in the context of regulation of the TCA cycle and guard cell metabolism.

2. REFERENCES

AZOULAY-SHEMER, T; PALOMARES, A; BAGHERI, A; ISRAELSSON-NORDSTROM, M; ENGINEER, C. B; BARGMANN, B. O. R; STEPHAN, A. B; SCHROEDER, J. I. **Guard cell photosynthesis is critical for stomatal turgor production, yet does not directly mediate CO_2-and ABA-induced stomatal closing**. The Plant Journal, v. 83, n. 4, p. 567-581, 2015.

GEMEL, J; RANDALL, D. D. **Light regulation of leaf mitochondrial pyruvate dehydrogenase complex: role of photorespiratory carbon metabolism**. Plant Physiology, v. 100, n. 2, p. 908-914, 1992.

HASSIDIM, M; DAKHIYA, Y; HUSSIEN, D; SHOR, E; ANIDJAR, A; GOLDBERG, K; GREEN, R. M. **CIRCADIAN CLOCK ASSOCIATED1 (CCA1) and the circadian control of stomatal aperture**. Plant Physiology, v. 175, n. 4, p. 1864-1877, 2017.

HEATH, O. V. S; RUSSELL, J. **Studies in Stomatal Behaviour: VI. AN INVESTIGATION OF THE LIGHT RESPONSES OF WHEAT STOMATA WITH THE ATTEMPTED ELIMINATION OF CONTROL BY THE MESOPHYLL**. Journal of Experimental Botany, v. 5, n. 2, p. 269-292, 1954.

HUMBLE, G. D; RASCHKE, K. **Stomatal opening quantitatively related to potassium transport: evidence from electron probe analysis**. Plant Physiology, v. 48, n. 4, p. 447-453, 1971.

KOSTAKI, K; COUPEL-LEDRU, A; BONNELL, V. C; GUSTAVSSON, M; SUN, P; McLAUGHLIN, F. J; FRASER, D. P; McLACHLAN, D. H; HETHERINGTON, A. M; DODD, A. N; FRANKLIN, K. A. **Guard cells integrate light and temperature signals to control stomatal aperture.** Plant Physiology, v. 182, n. 3, p. 1404-1419, 2020.

MCADAM, S. A. M; BRODRIBB, T. J. **The evolution of mechanisms driving the stomatal response to vapor pressure deficit**. Plant Physiology, v. 167, n. 3, p. 833-843, 2015.

MCDONALD, A. E; VANLERBERGHE, G. C. **The organization and control of plant mitochondrial metabolism**. Annual Plant Reviews online, p. 290-324, 2018.

MEDEIROS, D.B; PEREZ SOUZA L; ANTUNES W. C; ARAÚJO W. L; DALOSO D. M; FERNIE, A. R. **Sucrose breakdown within guard cells provides substrates for glycolysis**

and glutamine biosynthesis during light-induced stomatal opening. Plant Journal 94: 583–594, 2018.

OUTLAW, W. H. **Critical examination of the quantitative evidence for and against photosynthetic CO_2 fixation by guard cells**. Physiologia Plantarum, v. 77, n. 2, p. 275-281, 1989.

SHIMAZAKI, K. I; DOI, M; ASSMANN, S. M; KINOSHITA, T. **Light regulation of stomatal movement**. Annual review of plant biology, *58*(1), 219-247, 2007.

TARDIEU, F; SIMONNEAU, T. **Variability among species of stomatal control under fluctuating soil water status and evaporative demand: modelling isohydric and anisohydric behaviours**. Journal of experimental botany, p. 419-432, 1998.

WANG, Y; HILLS, A; BLATT, M. R. **Systems analysis of guard cell membrane transport for enhanced stomatal dynamics and water use efficiency**. Plant Physiol.164:1593–99, 2014.

WILLMER C, FRICKER M. ***Stomata***. London: Chapman & Hall, 1996.

SECOND PART - PAPER

PAPER - ^{13}C-positional isotope labelling analysis revealed a different mode of ^{13}C-distribution throughout the TCA cycle and glutamine synthesis in guard cells: a meta-analysis study

ABSTRACT

The tricarboxylic acid (TCA) cycle provides substrates for numerous metabolic pathways in prokaryotes and eukaryotes. In plants, the regulation of respiration assumes a higher level of complexity given that it is tightly coupled to photosynthesis. However, several TCA cycle enzymes, plus the mitochondrial pyruvate dehydrogenase (PDH), have been shown to be inhibited by light in leaves, which leads to a restricted carbon flux throughout leaf TCA cycle and glutamate/glutamine (Glu/Gln) synthesis during the day. Nonetheless, evidence suggests that in guard cells (GCs) both glycolysis and the TCA cycle are active in the light, most probably as a mechanism to support the synthesis of stomatal movement regulators, such as ATP, malate (Mal) and fumarate (Fum), as well as Gln. It seems reasonable to hypothesize, therefore, that guard cell TCA cycle is differentially regulated in the light, as compared to mesophyll cells (MCs). Here we have established a gas chromatography coupled to mass spectrometry-based ^{13}C-positional isotope labelling approach to investigate the ^{13}C distribution derived from phospho*enol*pyruvate carboxylase (PEPc) activity throughout the TCA cycle and associated pathways. This approach allowed the tracking of the incorporation of ^{13}C from PEPc activity into Mal, Glu and Gln. We then performed a multi-species/cell types meta-analysis of previous metabolic flux studies aiming to compare the ^{13}C distribution throughout the TCA cycle and associated pathways in GCs with those observed in MCs of C3 (MC-C3) or C4 (MC-C4) plants, as well as with sink or source MC-C3. In general, GCs ^{13}C distribution did not resemble those observed in MC-C4 or MC-C3 and showed similarities with sink MC-C3. Surprisingly, the ^{13}C incorporation into Mal derived from PEPc CO_2 fixation was higher in MC-C3 than in GCs. All tissues showed a high ^{13}C-enrichment in pyruvate (Pyr), being rapidly fully labelled in GCs under ^{13}C-Suc and in MC-C3 and MC-C4 under $^{13}CO_2$. However, the metabolic fluxes derived from Pyr were substantially different among GCs and MCs. Whilst GCs showed lower ^{13}C-enrichment in alanine (Ala), the ^{13}C-incorporation into Gln derived from PEPc, PDH and the TCA cycle was much higher in GCs than in both MC-C3 and MC-C4. Similarly, sink MC-C3 had 3-fold higher ^{13}C-enrichment in Gln than source MC-C3 under ^{13}C-Suc. Despite this similarity with sink MC-C3, only GCs

showed an increment of the fragment *m/z* 118 in Gln, which refers to the M1 isotopologue derived from PEPc fixation. Interestingly, increased Glu *m/z* 118 was observed in wild type (WT) Arabidopsis MCs when they were fed with ^{13}C-Pyruvate (^{13}C-Pyr), but not with ^{13}C-Glucose (^{13}C-Glc) or ^{13}C-Malate (^{13}C-Mal). However, increased Glu *m/z* 118 was observed in both *trxo1* mutant and *ntra ntrb* double mutant under ^{13}C-Glc. These results strongly suggest that PDH activity severely limits the glycolytic fluxes toward Glu/Gln synthesis in the light, which is due to the deactivation of this enzyme by phosphorylation and probably by a negative thioredoxin-mediated redox regulation. Collectively, our results highlight the effectiveness of our ^{13}C-positional isotope labelling approach and indicate a higher use of the carbon fixed by PEPc to Gln synthesis in GCs, compared to MC-C3 or MC-C4. The results are discussed in the context of regulation of TCA cycle and Glu/Gln synthesis.

Key words: Guard cell metabolism, metabolic fluxes, metabolic regulation, tricarboxylic acid cycle, thioredoxin-mediated redox regulation, glutamine.

Introduction

Respiration is a fundamental process for living organisms and it is separated in three main steps, namely glycolysis, the tricarboxylic acid (TCA) cycle and the mitochondrial respiratory chain (Krebs & Johnson, 1937; Beevers, 1961). In animals and most microorganisms, respiration is responsible for most of the cellular energy produced. In plants, this task is also accomplished by the photosynthetic process under light conditions. Thus, plant energetic metabolism has a higher level of complexity, in which a tight regulation between photosynthetic and (photo)respiratory metabolisms is observed (Møller & Rasmusson, 1998; Buchanan, 2016; Obata *et al.*, 2016; Souza *et al.*, 2018b). For instance, whilst the enzymes of the Calvin-Benson cycle are activated in the light, by a mechanism dependent of the ferredoxin-thioredoxin plastidial system (Buchanan, 2017), it has been recently shown that the non-plastidial thioredoxin system deactivates key enzymes of the mitochondrial (photo)respiratory metabolism (Balmer *et al.*, 2004; Yoshida & Hisabori, 2014, 2016; Daloso *et al.*, 2015b; Reinholdt *et al.*, 2019a; Fonseca-Pereira *et al.*, 2020). Furthermore, other post-translational regulation mechanisms such as phosphorylation and lysine acetylation of pyruvate dehydrogenase (PDH) and enzymes of the TCA cycle are also key points that negatively regulate the carbon fluxes toward the TCA cycle in the light (Tovar-Méndez *et al.*, 2003; Tcherkez *et al.*, 2005; Finkemeier *et al.*, 2011; Nunes-Nesi *et al.*, 2013). However, despite outstanding advances in the understanding of the regulatory mechanisms and the metabolite channelling via metabolon between the enzymes of the TCA cycle (Nietzel *et al.*, 2017; Zhang *et al.*, 2017, 2018; Fernie *et al.*, 2018), it remains not completely understood how the fluxes through this cycle are regulated.

Among the metabolic pathways that depend on carbon from respiratory intermediates, the synthesis of Glu, Gln and associated amino acids depends on the activity of the C6-branch of the TCA cycle (Araújo *et al.*, 2013). This idea is based on the fact that antisense or pharmacological inhibition of citrate synthase (CS), isocitrate dehydrogenase (IDH) or 2-oxoglutarate dehydrogenase (OGDH) alters substantially the amount of Glu and Gln produced in leaves (Araujo *et al.*, 2008; Sienkiewicz-Porzucek *et al.*, 2010; Sulpice *et al.*, 2010). However, given that the fluxes toward the TCA cycle are inhibited in the light, the source of carbon for Glu and Gln synthesis remained mysteriously unanswered until recently. Important information that partially fulfil this gap was provided by a diel course genome scale metabolic model which predicted that previous night-stored organic acids, especially citrate, would be

an important source of carbon to feed the C6-branch of the TCA cycle in the light (Cheung *et al.*, 2014). According to this model and in agreement with several other studies, plant TCA cycle does not seem to work as a cycle (Sweetlove *et al.*, 2010). Indeed, several non-cyclic flux modes have been demonstrated in leaves and seed embryos (Hanning & Heldt, 1993; Tcherkez *et al.*, 2005, 2009; Schwender *et al.*, 2006; Alonso *et al.*, 2007; Allen *et al.*, 2009; Gauthier *et al.*, 2010), which highlights the complexity of the regulation of the TCA cycle in plants.

Detailed information regarding the metabolic fluxes throughout the TCA cycle has been obtained by both mass spectrometry (MS) and nuclear magnetic resonance (NMR)-based ^{13}C-metabolic flux analyses (Zamboni *et al.*, 2009; Kim *et al.*, 2010; Heise *et al.*, 2014). NMR has great advantage over MS approaches given that it allows the analysis of the ^{13}C incorporation at specific atom position. However, NMR sensitivity is much lower than MS, which limits the use of NMR for small metabolic networks (Ratcliffe & Shachar-Hill, 2006; Antoniewicz, 2013). Thus, the establishment of a MS-based platform to analyse positional ^{13}C-isotope labelling offer the possibility to improve the resolution of metabolic flux analysis. Positional ^{13}C-isotope labelling analysis allows the discrimination of which pathways mostly contribute to the synthesis of a particular metabolite or to the activation of a metabolic pathway. For instance, ^{13}C-NMR has been recently used to investigate the source of carbon for Glu synthesis in leaves under $^{13}CO_2$. The results showed a specific ^{13}C incorporation into the carbon 1 of Glu, whilst no ^{13}C-enrichment was observed in the carbons 2 to 5 of the molecule (Abadie *et al.*, 2017). This indicates that there is incorporation of one carbon from the anaplerotic CO_2 assimilation catalysed by phospho*enol*pyruvate carboxylase (PEPc) activity into Glu and that no carbon from glycolysis, which is derived from the CO_2 fixed by ribulose-1,5-bisphosphate carboxylase/oxygenase (RubisCO), is incorporated into Glu under short time $^{13}CO_2$ labelling (Abadie *et al.*, 2017). Interestingly, whilst these results confirm predictions from previous metabolic models (Cheung *et al.*, 2014), they are in contrast to results from ^{13}C-isotope labelling experiments in guard cells (GCs) (Daloso *et al.*, 2015a, 2016; Robaina-Estévez *et al.*, 2017; Medeiros *et al.*, 2018). Therefore, it remains unclear whether the metabolic fluxes toward the TCA cycle and Glu/Gln synthesis in the light are differentially regulated in mesophyll (MCs) and GCs.

GCs are specialized cell types that surround the stomatal pore (Lima *et al.*, 2018a). Changes in guard cell metabolism regulate stomatal opening, which is an important process for the regulation of photosynthesis and transpiration (Lawson & Vialet-Chabrand, 2018).

GCs are known to have few chloroplasts and low chlorophyll content (Willmer & Fricker, 1996), which result in a lower photosynthetic capacity when compared to MCs (Gotow *et al.*, 1988; Lawson *et al.*, 2003). However, GCs have higher number of mitochondria and higher respiration rate (Willmer & Fricker, 1996; Araújo *et al.*, 2011a). Therefore, it is reasonable to assume that mitochondrial metabolism is the main source of ATP for these cells. However, this assumption implicates that mitochondrial respiratory metabolism should be active in the light, by contrast of that observed in MCs. Indeed, recent ^{13}C-sucrose (^{13}C-Suc) labelling study suggests a particular regulation of both glycolysis and the TCA cycle in GCs in the light (Medeiros *et al.*, 2018). However, a detailed comparison of the metabolic fluxes throughout the TCA cycle between GCs and MCs is still missing. Here we have established a gas chromatography coupled to mass spectrometry-based (GC-MS) ^{13}C-positional isotope labelling approach to investigate the distribution of the carbon fixed by PEPc into Mal, Glu and Gln. After establishing this approach, we performed a meta-analysis of previously published data from ^{13}C-isotope labelling experiments carried out in MCs of Arabidopsis C3 (MC-C3) and maize C4 (MC-C4) and sink and source leaves of Arabidopsis plants and in GCs of Arabidopsis and tobacco. Collectively, our results indicate that the fluxes from glycolysis and PEPc activity toward Gln synthesis are higher in GCs when compared with those observed in MC-C3 or MC-C4, suggesting a differential regulation of both glycolysis and the TCA cycle in GCs. Notwithstanding, our results indicate that the light-dependent inhibition of PDH severely restricts the fluxes of carbon through Glu synthesis. The results are discussed in the context of regulation of the TCA cycle and guard cell metabolism.

Material and methods

Data set acquisition

Chromatograms of published works were kindly provided by their authors (Table S1). The data set comprised 320 chromatograms of primary metabolites identified by GC-TOF-MS from Arabidopsis rosettes, Arabidopsis and maize leaves and from guard cell-enriched epidermal fragments of Arabidopsis and tobacco. Details of the data set used in this work are found in the Table S1. In the following sections we describe the general methodologies employed in the experiments used by the respective works for the collection of the metabolite data.

Plant material and growth condition

Arabidopsis thaliana, accession Columbia-0, was grown in 6-cm-diameter pots, under 8/16-h day/night cycles at an average irradiance of 120 μmol m^{-2} s^{-1}, temperatures of 22-20°C (day)/20-18°C (night), and 50% relative humidity and CO_2 concentration around 420 ppm. Fully expanded rosettes of 5-week-old plants, or paired leaves of single plant rosettes, were harvested and used for feeding experiments using $^{13}CO_2$ or ^{13}C-Suc and for the isolation of guard cell-enriched epidermal fragments, which were subsequently used for ^{13}C-Suc or ^{13}C-$NaHCO_3$ labelling experiments.

Nicotiana tabacum (L.) seeds were germinated in Petri dishes containing MS medium (Murashige & Skoog 1962) and cultivated *in vitro* for 15 days. Seedlings were transplanted to 0.1 L pots containing Plantimax® substrate, cultivated for 15 days under photoperiod of 14 h illumination and light intensity of 120 mol m^{-2} s^{-1} and, then, transferred to 20 L pots under greenhouse conditions. Completely expanded and non-senescent leaves of non-flowering 3 to 4-months-old plants were used for the preparation of guard cell-enriched epidermal fragments, which were subsequently used for ^{13}C-$NaHCO_3$ labelling experiments.

Maize (*Zea mays* L. cv. B73) seeds were germinated in darkness in Petri dishes on moistened filter paper (3 d, 28 °C), then transferred to 10-cm-diameter pots, grown for 5 d under 16/8 h day/night cycles (irradiance 105 μmol photons m^{-2} s^{-1}, 22/18 °C, 70% relative humidity) and, finally, under 14/10 h day/night cycles (irradiance 480 μmol photons m^{-2} s^{-1}, 25/22 °C, 65% relative humidity). Leaves of 3-weeks-old plants were used for $^{13}CO_2$ labelling experiments.

^{13}C-isotope kinetic labelling experiments in whole plant Arabidopsis and in leaves of Arabidopsis and maize

$^{13}CO_2$ feeding experiment of Arabidopsis rosettes was performed by providing a gas mixture (concentration of 78% N_2, 21% O_2, 400 ppm $^{13}CO_2$ and flow of 5 liters min^{-1}) inside of a 380 mL-transparent labelling chamber (Magenta GA-7 plant culture box), illuminated with a photon flux density of 115 μmol m^{-2} s^{-1} by a FL-460 lighting unit from Walz. Individual plants in their pots were quickly moved from the growth chamber to the labelling chamber (<5 s) and quenched at different times after the start of labelling. Metabolism was

quenched directly in the chamber by pouring a large volume of liquid nitrogen over the rosette through a funnel placed through a small outlet in the box. All frozen plant material above the plastic foil was harvested and stored at -80°C.

^{13}C-Suc feeding experiment of Arabidopsis leaves was performed by petiole feeding assay. The leaf lamina of the "feeding" leaf was removed by a clear scalpel cut and a reservoir containing labelling solution (30 µL of ^{13}C-suc in tap water) was immediately placed to cover the petiole stump of the remaining petiole that was still attached to the plant. The solution covered the cut completely and entered the plant via the petiole. P1–P7 or P1–P9 leaves, in the fresh mass range of 2.5–50.0 mg, were harvested from each rosette and metabolically inactivated by shock freezing in liquid nitrogen.

$^{13}CO_2$ feeding experiment of maize plants was performed by providing a gas mixer (78% N_2, 21% O_2, and 420 ppm $^{12}CO_2/^{13}CO_2$) into a custom-designed labelling chamber of 320 ml volume. Flow at 10 L min^{-1} was used for pulses of up to 1 min, and 5 L min^{-1} for longer pulses. The chamber was made of copper with a hollow body and a transparent Plexiglas lid with a hollow vertical tube (internal diameter ~2cm) sealed with transparent film (Toppits©) and illuminated with 480 µmol photons m^{-2} s^{-1} by an external lamp (FL-460 Lighting Unit, Walz, Effeltrich, Germany). Plant material was quenched by dropping a pre-cooled (in liquid N_2) copper rod with a sharp machined edge down the hollow tube in the lid into the labelling chamber, freeze-clamping a leaf disc (1.9 cm diameter, ~65 mg FW) between this rod and another copper rod fixed in the chamber, protruding into the base of the chamber and extending well below the outside of the chamber to allow pre-cooling with liquid N_2. Labelling started 2h after the start of the light period, to ensure metabolic steady state, and harvested at different times after starting labelling. Leaf discs from two plants were pooled per time point.

Guard cell isolation

A pool of guard cell-enriched epidermal fragments (simply referred here as guard cells) were isolated following a protocol that was recently optimized for metabolite profiling analyses (Daloso *et al.*, 2015a). Briefly, guard cells were isolated from pre-dawn harvested samples by blending approximately 5 Arabidopsis rosettes per replicate, or 2 fully expanded tobacco leaves, in a Warring blender (Philips, RI 2044 B.V. International Philips, Amsterdam, The Netherlands), incorporating an internal filter to remove excess mesophyll cells, fibres and

other cellular debris. All guard cell isolations were carried out in the dark in order to maintain closed stomata and simulate opening, following the natural circadian rhythm.

^{13}C-isotope kinetic labelling experiment in guard cells

After isolation, guard cells were transferred to light or dark conditions and incubated in a solution containing 50 µM $CaCl_2$ and 5 mM MES-Tris, pH 6.15 in the presence of 5.0 mM ^{13}C-$NaHCO_3$ (Arabidopsis) or in a solution containing 10 mM KCl, 50 µM $CaCl_2$ and 5 mM MES– TRIS, pH 6.15 in the presence of 0.1 mM ^{13}C-Suc (Tobacco). The experiment was initiated at the beginning of the day light period. Guard cell samples were rapidly harvested on a nylon membrane (220 µm) and snap-frozen in liquid nitrogen under dark condition or after different times of light exposure and finally stored at -80°C before subsequent metabolic analyses.

Metabolomics analysis

GCs, leaves or Arabidopsis rosettes were ground to a fine powder using a Retsch ball-mill. Metabolites were extracted from ~50-to-100 mg (fresh weight) of frozen plant powder. Metabolites extraction and their derivatization were carried out exactly as described by Lisec *et al.*, (2006). Briefly, metabolite extraction was performed in methanol, with shaking at 70°C for 1 h. Ribitol (60 µl, 0.2 mg mL^{-1}) was added as internal standard. Following centrifugation, the supernatant was taken and the polar and apolar phases were separated by adding chloroform and deionized water to the tube. A new centrifugation was performed and 150 µL or 1 mL of the polar (upper) phase of leaves and GCs, respectively, was taken and reduced to dryness. Metabolites were derivatized by methoxyamination, with subsequent addition of tri-methyl-silyl (TMS) and finally analysed by GC-EI-TOF-MS, as detailed in Lisec et al. (2006).

Establishment of the ^{13}C-positional isotope labelling approach

In order to investigate the ^{13}C-positional isotope labelling in metabolites of, or associated to, the TCA cycle, we first searched for fragments of the metabolites of this pathway from metabolomics data derived from a well-established gas chromatography-electron impact- *time of flight*-mass spectrometry (GC-EI-TOF-MS) platform (Lisec *et al.*, 2006) and also from studies involving TMS-derivatization. We further revisited the Golm Metabolome Database to identify the chemical structure of the TMS-derivatized compounds

of interest and also reviewed the literature, aiming to find which carbons are included in each molecule fragment obtained from electron impact (EI) fragmentation of TMS-derivatized compounds. We searched the pattern of EI-mediated fragmentation of metabolites belonging to the groups of amino acids, organic acids and sugars (Dejongh *et al.*, 1969; Petersson, 1972; Leimer *et al.*, 1977; Antoniewicz *et al.*, 2007; Abadie *et al.*, 2017; Souza *et al.*, 2018a; Okahashi *et al.*, 2019). In parallel, an *in silico* analysis was performed to identify the major well-known fragmentation patterns resulting from EI ionization using the software ChemBioDraw 12.0 (CambridgeSoft, Cambridge, MA, USA). Finally, a small EI-based fragmentation map of TMS compounds was assembled, containing the estimated cleavage groups and resulting carbon skeletons for each metabolite of interest. Here we only present the results from metabolites associated to the TCA cycle, following the focus of the study.

Determination of the ^{13}C-enrichment in metabolites associated to the TCA cycle

We revisited 320 chromatograms/mass spectra, identified and selected seven metabolites of interest (Pyr, Ala, Mal, Fum, succinate, Glu and Gln) in all tissue types, although not all metabolites were found in every work (Table S1), and analysed the ^{13}C-enrichment in these metabolites. We determined the relative isotopomer abundance (%) of the isotopologues (M, M1, M2…Mn) and the total ^{13}C-enrichment was calculated as described previously (Lima *et al.*, 2018b), by assuming the multiplication of the relative isotopomer abundance of the isotopologues by the number of ^{13}C atoms incorporated in each isotopomer (M0*0+M1*1+M2*2…Mn*n) and then dividing by the number of C of the molecule. Given that experiments had different labelling times, we also determined the total ^{13}C-enrichment per min, dividing the total ^{13}C-enrichment obtained at the last time-point by the ^{13}C-enrichment at time 0 and then normalizing the data by the experiment labelling time. We are aware that the ^{13}C incorporation into metabolites is not linear and that our results may not reflect the real rate of ^{13}C incorporation min^{-1}. Thus, our comparisons of the total ^{13}C-enrichment min^{-1} obtained from experiments performed with different ^{13}C labelling times should be taken with caution. Yet, we found this approach worth to use for the comparison between GCs and MCs subjected to 60 minutes of labelling.

Statistical analysis

All data are expressed as mean ± standard error (SE). Data from different experiments were compared using ANOVA and Dunnet's test ($P < 0.05$). Exception is made for the data

from MC-C4 experiment, which contained only one biological replicate and, thus, did not allowed the calculation of averages and SEs, as well as a statistical comparison to other experiments. Punctual comparisons of GCs with MC-C3 and with source or sink MC-C3 were carried out by Student's *t*-test ($P < 0.05$), as indicated in the legend of each figure. All statistical analyses were performed using Sigma Plot 12® (Systat Software Inc., San Jose, CA, USA).

Results

Establishment of the GC-EI-TOF-MS-based ^{13}C-positional isotope labelling approach

To identify the ^{13}C-positional isotope labelling in different metabolites, we established a GC-EI-TOF-MS-based approach to investigate the distribution of the carbon fixed by PEPc over metabolites of, or associated to, the TCA cycle. Similar strategy has been used to analyse positional isotope labelling in metabolites associated to photorespiration (Souza *et al.*, 2018a). Here, we first assemble a map of fragmentation of metabolites associated to the TCA cycle, which includes TCA cycle intermediates, Pyr and amino acids (Figure 1). This was obtained by reviewing literature and the Golm Metabolome Database to identify chemical structures of TMS-derivatized compounds and metabolite fragmentation patterns. Then, we performed an *in silico* simulation of metabolite fragmentation using the software ChemBioDraw. For instance, after EI-based fragmentation of the Glu 3TMS, the mass-to-charge (*m/z*) ratio 246 is the fragment that shows the highest intensity and that has been widely suggested to contain the carbons 2, 3, 4 and 5 of the Glu backbone (Leimer *et al.*, 1977; Huege *et al.*, 2007). We then reproduced this fragmentation using ChemBioDraw and estimated that Glu and Gln are cleaved at the TMS-carboxyl group in the carbon 1 position, resulting in two major fragments namely *m/z* 117 and *m/z* 246 for Glu, and *m/z* 117 and *m/z* 245 for Gln (Figure 1). Since the incorporation of ^{13}C atoms in a fragment causes a shift in the *m/z* ratio observed in the mass spectra (Okahashi *et al.*, 2019), we deduced that after ^{13}C-labelling the Glu fragment *m/z* 117 should change to 118 and the fragment *m/z* 246 should range from 246 to 250, according to the number of labelled carbons incorporated. Acknowledging a recent ^{13}C-NMR metabolic flux study that indicates that the carbon 1 position of both Glu and Gln is derived from PEPc activity (Abadie *et al.*, 2017), we considered that the fragment *m/z* 117 carries the carbon 1 position of both Glu and Gln and, most important, that this carbon is derived from PEPc

fixation, rather than from acetyl-CoA, as a product of PDH activity, or from the TCA cycle (Figure 2). Thereafter, we used the analysis of ^{13}C-enrichment in *m/z* 246, *m/z* 245 and *m/z* 117 fragments to distinguish the relative contribution of glycolysis and TCA cycle pathways (*m/z* 246 and *m/z* 245) from that of the CO_2 fixation via PEPc (*m/z* 117) to the synthesis of Glu and Gln.

We repeated this same strategy for each major fragment of other metabolites associated with the TCA cycle. Interestingly, *m/z* 117 is a common fragment obtained after EI-fragmentation of metabolites of the TCA cycle (see Mal *m/z* 117 in the Figure 1 and the blue identification in the Figure 2, which represent fragments with *m/z* 117). Taking in consideration recent studies showing that the carbon assimilated by PEPc is directly incorporated into the carbon 4 of oxaloacetate (OAA) and subsequently incorporated into the carbon 4 of Mal (Abadie *et al.*, 2017), and that the fragments *m/z* 117 and *m/z* 233 contains, respectively, the carbon 4 and the carbons 2, 3 and 4 of the Mal backbone (Okahashi *et al.*, 2019), we thus used the *m/z* 117 fragment to investigate the ^{13}C enrichment in Mal as an indirect product of PEPc fixation (Figure 3). The GC-EI-TOF-MS-based ^{13}C-positional isotope labelling approach developed in this work showed that the analysis of the ^{13}C-enrichment in the fragment *m/z* 117, through the increase in the intensity of *m/z* 118, represents an indirect and effective tool to measure PEPc activity *in vivo*.

^{13}C-isotopomer relative abundance analysis

In order to facilitate comparisons with GCs and considering that great portion of the leaf is composed by MCs, the results of ^{13}C-feeding experiments performed in leaves are described as MC-C3 (for C3 plants) and MC-C4 (for C4 plants). Given the similarity in the labelling time used in some ^{13}C-feeding experiments, we first compared the metabolism of MC-C3 and MC-C4 under $^{13}CO_2$ with that of GCs under ^{13}C-Suc or ^{13}C-HCO_3. For this, we analysed total ^{13}C-enrichment, metabolite levels and relative isotopomer abundance of Pyr, which is the end-product metabolite of glycolysis, and of the TCA cycle-intermediates succinate (Succ), Fum and Mal. In addition, we analysed three amino acids whose biosynthetic pathways are associated to the TCA cycle. These amino acids are Glu and Gln, which depends on carbon derived from 2-oxoglutarate (2-OG), and Ala, that is synthetized through alanine aminotransferase (AlaAT) using Pyr as substrate.

MC-C4 showed a large increase in the isotopomer M4 (*m/z* 249) of Fum under $^{13}CO_2$, reaching maxima of 38 % at 40 minutes, when then it decreased towards 60 min. GCs had

increases in M2 (*m/z* 247) over time, whilst both M3 (*m/z* 248) and M4 (*m/z* 249) showed slight increases after 16 mins under ^{13}C-HCO_3 (Figure 4). By contrast, Fum labelling pattern in MC-C3 was highly stable under $^{13}CO_2$ over time, with slight increases in M3 and M4 at 60 min. The decline in Fum M (*m/z* 245) and the labelling patterns of M1-M4 indicate that Fum was fully labelled in all tissues analysed, although MC-C4 was labelled with less time, followed by GCs and MC-C3, subsequently. The results of the relative isotopomer abundance of the Mal *m/z* 233 fragment was similar to those observed for Fum *m/z* 245, especially in MC-C4. MC-C3 had a 12 %-increase in M3 (*m/z* 236) after 60 minutes of light exposure, whilst GCs increased ~6% in M1 (*m/z* 234), M2 (*m/z* 235) and M3 (*m/z* 236) after 40 minutes of light exposure. GCs had lower M values of Fum than Mal at 60 min, and the opposite was observed in MC-C3, which, in this case, was due to a higher increase in both M3 and M4 of Fum from 20 to 60 min (Figure 4). Interestingly, the labelling of the carbon 4 of Mal, analysed here through the relative increase of *m/z* 118, raised linearly up to 26% at 60 min in MC-C3, highlighting a higher incorporation of ^{13}C derived from PEPc in Mal over time. As expected, MC-C4 showed a rapid and the highest increase (46% at 40 min) in this isotopomer, while GCs showed an intermediate increase (25 % at 40 min). Succ was similarly labelled in MC-C4 and GCs, whilst it was not detected in MC-C3 samples (Figure 4).

Pyr and Ala were not detected in GCs under ^{13}C-HCO_3. The comparison of these metabolites between GCs and MCs was then based in results from GCs under ^{13}C-Suc. Pyr was rapidly fully labelled in all tissues, in which M3 (*m/z* 177) reached maxima of 36, 73 and 48 % in MC-C3, MC-C4 and GCs, respectively (Figure 5). A similar labelling pattern was observed in Ala in MC-C3 and MC-C4, but GCs showed much lower increase in M2 and decrease in M over 60 min (Figure 5). These results indicate that Pyr is rapidly fully labelled in MCs and GCs, but this carbon is rapidly transferred to Ala through AlaAT only in MC-C3 and MC-C4 (Figure 5).

We next evaluated the relative isotopomer abundance in Glu and Gln, two amino acids that are potential fates for carbons derived from Pyr. In this analysis, we only detected Glu *m/z* 246 in GCs under ^{13}C-HCO_3, but all isotopomers of Glu *m/z* 246, Glu *m/z* 117, Gln *m/z* 245 and Gln *m/z* 117 were detected in GCs under ^{13}C-Suc and MC-C3 and MC-C4 under $^{13}CO_2$ (Figure 6). GCs under ^{13}C-Suc showed the highest decrease in Glu *m/z* 246 (M) (reaching 35 % at 60 min) and increase in Glu *m/z* 248 (M2) (reaching 27 % at 60 min) (Figure 6), suggesting a fast incorporation of two carbons into this metabolite, which can be derived from the TCA cycle or from acetyl-CoA (AcCoA) produced by PDH activity (Figure

2). Increases in Glu *m/z* 249 (M3) and Glu *m/z* 250 (M4) in GCs under ^{13}C-Suc were also observed. GCs under ^{13}C-HCO_3 showed a slight decrease in M over time, and a slight increase in both M3 and M4 of Glu from 32 to 40 min (Figure 6). MC-C4 also have a decrease in Glu *m/z* 246 (M) over time, with slight increases in M2, M3 and M4 of Glu after 20 min. MC-C3 had no expressive changes in the isotopomers of Glu *m/z* 246, in which an increase of 3% in M2 was observed, while M3 and M4 increased 1.8% and 0.44% (Figure 6).

The relative isotopomer abundance of the Glu *m/z* 118 did not change in MC-C3 and was slightly increased (3.9 %) in MC-C4 over time. In contrast, GCs had a 19%-increase in Glu *m/z* 118 (M1) (Figure 6). No ^{13}C enrichment in Gln *m/z* 245 of MC-C3 and in Gln *m/z* 117 of MC-C4 was observed. Gln *m/z* 245 was slightly labelled in MC-C4, while a rapid and large increase (31%) in M3 (*m/z* 248) and M4 (*m/z* 249) coupled to a linear decrease in M (*m/z* 245) in GCs under ^{13}C-Suc was observed (Figure 6). These results indicate that MC-C3 have null or minimum ^{13}C incorporation of carbons from $^{13}CO_2$ into Glu and Gln in the light, with a maximum of 2 carbons being incorporated into Glu but not in Gln under this condition (Figure 7). By contrast, the carbons from ^{13}C-Suc were rapidly incorporated into the fragment *m/z* 246 of Glu in GCs, that contains the carbons 2, 3, 4 and 5 of the Glu backbone (Figure 7). The higher increase in M2 than in M3 and M4 in GCs under ^{13}C-Suc suggests a higher contribution of the TCA cycle or of PDH to this labelling pattern of Glu. In this vein, the absence of ^{13}C enrichment in Mal, Fum or Succ under ^{13}C-Suc (Figure 7) strongly suggests a great contribution of PDH for Glu labelling in GCs. Furthermore, only GCs showed clear increases in Glu and Gln *m/z* 118, indicating that this metabolite is fully labelled in GCs in the light by carbons coming from glycolysis, the TCA cycle and PEPc (Figure 7). Finally, no ^{13}C derived from PEPc was incorporated into Gln in both MC types, highlighting a specific labelling pattern of these metabolites in GCs.

Total ^{13}C-enrichment analysis

The previous isotopomer analysis highlights how many carbons have been incorporated into each metabolite from the labelled substrate over time and the velocity of this incorporation. We next calculated the total ^{13}C-enrichment found in each metabolite. The data presented are normalized by the total ^{13}C-enrichment found at the time 0 of each experiment (Figures 8-10). No ^{13}C-enrichment in Mal, Fum and Succ in GCs under ^{13}C-Suc was observed. The total ^{13}C-enrichment in Mal (*m/z* 117 and *m/z* 233), Fum (*m/z* 245), Succ (*m/z* 247), Pyr (*m/z* 174) and Ala (*m/z* 116) was higher in MC-C4 than in both MC-C3 and GCs

(Figures 8,9). The total ^{13}C-enrichment in Fum *m/z* 245 and Mal *m/z* 233 increased in both GCs and MC-C3 over time, but GCs showed significant differences in Fum and Mal after 16 min and 24 min, respectively, while MC-C3 showed significant difference in these metabolites only at 60 min (Figure 8). Increased labelling in Succ *m/z* 247 in GCs under ^{13}C-HCO_3 was observed, reaching maxima of 17% at 32 minutes, when then decreased towards 40 min (Figure 8).

GCs showed a high total ^{13}C-enrichment in Pyr derived from ^{13}C-Suc, reaching 51% of increase at 60 min, whilst MC-C3 showed 45%-increase in Pyr at the same time point (Figure 9). The pattern and the magnitude of Ala labelling in MC-C3 and MC-C4 resembled those observed in Pyr in each of these cells. GCs also showed a significant increase in Ala total ^{13}C-enrichment over time. However, the magnitude of this increase was lower than that observed for Pyr (Figure 9). These results indicate that carbons photosynthetically fixed are highly directed to Pyr and Ala in both C3 and C4 MCs, while in GCs the carbon from ^{13}C-Suc is relatively lesser incorporated into Ala, as compared to Pyr. The total ^{13}C-enrichment in Glu *m/z* 246 observed in GCs under ^{13}C-HCO_3 resembled that observed in MC-C4. GCs under ^{13}C-Suc had the highest total ^{13}C-enrichment in Glu *m/z* 246 and Gln *m/z* 245. Gln had an ^{13}C-enrichment of 65.8% in the carbons 2 to 5 (*m/z* 246) after 60 min in the light (Figure 10). Regarding the carbon 1 of Glu and Gln (i.e. *m/z* 117), GCs had an increase of 37 and 26 % in the total ^{13}C-enrichment of Glu and Gln, respectively, while MC-C3 and MC-C4 showed slight changes over time, although the total ^{13}C-enrichment in MC-C3 at 60 min was statistically different from the time 0 (Figure 10).

Changes in metabolite content

We further analysed whether the level of metabolites changed over time. Fum content increased significantly only in GCs under both labelled substrates, but at greater extent under ^{13}C-Suc. Interestingly, Fum showed an accumulation peak in GCs at 10 and 24 min under ^{13}C-Suc and ^{13}C-HCO_3, respectively, when then its levels started to decrease (Figure 11). The changes in Mal content over time was similar to those of Fum in GCs under ^{13}C-Suc, with an accumulation peak at 10 min after light exposure. No statistical difference was found in the contents of Fum and Mal in MC-C3 over time. Similarly, Fum, Mal and Succ levels did not change substantially in MC-C4 over time and in GCs under ^{13}C-Suc Succ levels did not change either (Figure 11). However, in GCs under ^{13}C-HCO_3, Succ increased linearly until 24 min and then decreased towards 40 min (Figure 11). In MC-C3, no statistical difference was

found in the contents of Pyr, Ala, Glu and Gln over time. Pyr decreased, while no difference in Ala was observed in GCs. Both metabolites tended to decrease in MC-C4 (Figure 12). Notably, Glu and Gln increased only in GCs under ^{13}C-Suc. Whilst Glu showed an accumulation peak at 10 min, followed by a decrease in its content, Gln showed a progressive and large increase over time (Figure 13). In summary, GCs had large alterations in metabolite levels over time, whilst no significant change was observed in MC-C3. The reductions in Pyr levels and the accumulation of Gln over time in GCs suggest a possible connection among these pathways, as previously suggested by the ^{13}C analysis. Furthermore, the accumulation peaks observed in Fum and Succ suggest that these metabolites were degraded over time, as suggested by the total ^{13}C- enrichment of Succ *m/z* 247 under ^{13}C-HCO_3.

Total ^{13}C-enrichment per min analysis

Our previous results showed the incorporation of ^{13}C derived from PEPc activity into Mal of GCs under ^{13}C-HCO_3 and MCs of C3 and C4 plants under $^{13}CO_2$. We statistically compared the total ^{13}C-enrichment in Mal from MC-C3 and GCs at 60 and 40 min, respectively, which was higher in MC-C3 in both *m/z* 117 and *m/z* 233 fragments (Figure 14). MC-C4 had the highest rate of ^{13}C incorporation into Mal, suggesting a higher PEPc activity. Given that the labelling time used in MCs experiments was different from that used in the GCs experiment, we normalized the total ^{13}C-enrichment by the respective labelling time, *i.e.* 60 min for MCs and 40 min for GCs, generating the rate of enrichment, given as the total ^{13}C-enrichment min^{-1}. After data normalization, the total ^{13}C-enrichment min^{-1} in Mal *m/z* 117 was still significantly lower in GCs, whilst the rate of ^{13}C-enrichment in *m/z* 233 was slightly higher, suggesting a differential labelling pattern of the carbons 2 and 3 of the Mal backbone, when comparing MCs and GCs. Regarding the other metabolites of the study, GCs had a higher total ^{13}C-enrichment min^{-1} in Pyr, Fum and Gln and lower ^{13}C-enrichment min^{-1} in Ala, when compared to MC-C3 (Figure 15). In summary, the highest rates of total ^{13}C-enrichment in Pyr, Ala, Mal, Fum and Succ were observed in MC-C4, whilst GCs had the highest total ^{13}C-enrichment min^{-1} in Glu and Gln.

Sink and source Arabidopsis (C3) mesophyll cells under ^{13}C-sucrose

We further analysed chromatograms of sink and source MCs of Arabidopsis plants fed with ^{13}C-Suc for 240 min. The aim was to investigate the differences among sink and source MC-C3 and qualitatively compare them to GCs, which is believed to have several characteristics of sink cells. Our meta-analysis showed that there are strong differences

between the sink and source MC-C3 in regard to the total ^{13}C-enrichment of metabolites of, or associated to, the TCA cycle. For instance, sink MC-C3 showed higher total ^{13}C-enrichment in Mal, Fum and Succ than source MC-C3, although the levels of these metabolites were not different between these cell types. No statistical difference was found for total ^{13}C-enrichment and metabolite levels of Ala when comparing source and sink MC-C3, although source MC-C3 tended to show higher values for this metabolite. In contrast, the total ^{13}C-enrichment and metabolite levels of both Glu and Gln were higher in sink MC-C3. Comparatively, both GCs and sink MC-C3 showed a higher use of the carbon derived from ^{13}C-Suc to the synthesis of Glu and Gln. However, it is worth mention that the isotopomer analysis performed by Dethloff and collaborators showed the incorporation of only three carbons labelled into Mal and Fum and two into Glu, which would distinguish GCs from sink MC-C3 (Dethloff *et al*. 2017). Furthermore, sink MC-C3 had higher maltose content, but no ^{13}C-enrichment in this metabolite (Figure 16). This suggests starch degradation in sink MC-C3 and that this starch was most probably synthesized before ^{13}C-Suc feeding.

Insights into the source of carbon for Glu synthesis in C3 mesophyll cells

In order to obtain better insights into the source of carbon for Glu synthesis and whether the mitochondrial thioredoxin (TRX) system is involved in the regulation of this pathway, we revisited chromatograms of ^{13}C-feeding experiments carried out with MC-C3 from Arabidopsis wild type (WT), *trxo1* mutant and *ntra ntrb* double mutant fed with ^{13}C-Glc, ^{13}C-Mal or ^{13}C-Pyr. In WT plants, the total ^{13}C-enrichment min^{-1} in Pyr *m/z* 174 was higher under ^{13}C-Glc than under ^{13}C-Mal, highlighting that glycolysis is probably the major source of carbon for Pyr synthesis in MC-C3. Nevertheless, a significant ^{13}C-enrichment under ^{13}C-Mal was also observed, which indicates activity of the malic enzyme (ME) under this condition (Figure 17). As expected, Fum had higher total ^{13}C-enrichment min^{-1} under ^{13}C-Mal than under ^{13}C-Glc or ^{13}C-Pyr. However, no difference was observed in the total ^{13}C-enrichment min^{-1} in both Mal and Fum when comparing ^{13}C-Glc and ^{13}C-Pyr treatments. This suggests that the glycolytic fluxes toward Mal and Fum pass through Pyr, which is probably converted into OAA by the activity of Pyr carboxylase (PC) (Figure 17). Lastly, the total ^{13}C-enrichment min^{-1} in Glu *m/z* 246 is higher under ^{13}C-Pyr than under the other labelled substrates. Furthermore, ^{13}C-enrichment in Glu *m/z* 117 is only observed under ^{13}C-Pyr (Figure 17). These results suggest that the enhancement of PDH activity by increasing substrate availability (^{13}C-Pyr treatment) leads to higher enrichment in the Glu-fragments containing the carbons 1 (*m/z* 117) and 2-to-5 (*m/z* 246) of the Glu backbone.

We further analysed Glu *m/z* 117 in MC-C3 of plants lacking TRX *o1* or both NADPH-dependent thioredoxin reductases NTRA and NTRB (Figure 18). Under ^{13}C-Mal, no ^{13}C-enrichment in Glu *m/z* 117 was observed. Under ^{13}C-Pyr, we observed ^{13}C-enrichment in all genotypes but with no difference among them. However, when we analysed the data under ^{13}C-Glc, we observed significant ^{13}C-enrichment in Glu *m/z* 117 only in the mutants, with no difference between them (Figure 18). This result highlights that the PEPc-mediated incorporation into the carbon 1 of the Glu backbone is probably regulated by the mitochondrial NTR/TRX system (Figure 19). Taken together, the data presented here suggest that GCs have a particular mode of metabolic fluxes throughout the TCA cycle and associated pathways (Figure 20).

Discussion

Insights into *in vivo* PEPc activity and the source of carbon for Glu and Gln synthesis revealed by ^{13}C-positional isotope labelling

^{13}C-metabolic flux analysis (MFA) is an extremely powerful approach to unveil pathways activation, in comparison to other regular approaches that measure the accumulation of particular metabolites in a specific time (Ratcliffe & Shachar-Hill, 2006), particularly considering that metabolic fluxes do not necessarily correlate either with the accumulation of metabolites or with the level of transcripts and proteins of the pathway under investigation (Williams *et al.*, 2008; Fernie & Stitt, 2012; Szecowka *et al.*, 2013). However, although it may seem straightforward to perform, identifying the fate of the ^{13}C released by a certain labelled substrate and to identify the precise atom position of the ^{13}C incorporation are of the major challenges in plant metabolomics. This is particularly due to both the intrinsic complexity of plant cell metabolism and the technical limitations available for metabolomics. Given the possibility to identify ^{13}C-labelling at the level of atom position, ^{13}C- NMR is one of the best tools for MFA. However, NMR is less sensitive than MS (Silva *et al.*, 2016). This explains why NMR has not been used for guard cell MFA yet (Medeiros *et al.*, 2019), given that an enormous amount of guard cells would be required for such analysis. An alternative possibility to overcome this limitation and to improve guard cell MFA is the development of a method to determine positional isotope labelling in compounds identified by MS. In this context, the data from GC-EI-TOF-MS is extremely useful for the establishment of such method, given that it offers high resolution/sensibility with a stable fragmentation pattern due to the strong energy used in EI. However, the lack of a clear fragmentation map has hampered the analysis of ^{13}C-enrichment at different carbon positions within the molecule.

Here, aiming to overcome the technical limitations of MS-based MFA, and inspired by the works from Tcherkez group that have provided great contribution to our knowledge concerning the regulation of leaf TCA cycle and Glu synthesis by ^{13}C-NMR MFA, we created a fragmentation map of TCA cycle-related metabolites. This allowed us to investigate the ^{13}C distribution from PEPc activity into Mal, Glu and Gln. By following the intensity of the fragments *m/z* 117 and *m/z* 118, we could obtain insights into the ^{13}C incorporation into Mal, which indirectly refers to the *in vivo* PEPc activity. Moreover, we could investigate the contribution of glycolysis, the TCA cycle and PEPc activity for the synthesis of Glu and Gln. Our results are in close agreement with recent ^{13}C-NMR MFA. For instance, it has been shown that leaves under $^{13}CO_2$ and light conditions have a specific ^{13}C incorporation into the C1 of Glu, whilst no ^{13}C enrichment in the carbons 2-to-5 is observed (Abadie *et al.*, 2017). This indicates that one of the carbons incorporated into Glu comes from the anaplerotic CO_2 assimilation mediated by the activity of PEPc. Our results reinforce this hypothesis and highlight that GCs have much higher ^{13}C incorporation from PEPc into Glu and especially Gln in the light, as compared to MCs. We also showed that MC-C4 have higher ^{13}C incorporation into Mal derived from PEPc than MC-C3. These results highlight the effectiveness of our ^{13}C-positional isotope labelling approach, which can be further applied to establish a protocol to measure PEPc activity *in vivo* using GC-EI-MS data. Noteworthy the direct measurement of PEPc activity *in vivo* will require specific ^{13}C-experiments using ^{13}C-HCO_3 as labelled substrate and sample harvesting over a scale of seconds to minutes. An alternative approach for the determination of PEPc activity *in vivo* has been recently established by ^{13}C-NMR (Abadie & Tcherkez, 2019). Here, we provide the first evidence that this determination can also be achieved by an easier way, through data analysis of GC-EI-TOF-MS-based ^{13}C-isotope labelling studies. Additionally, it is important to highlight that this approach is not limited to plant cells, given that GC-EI-MS is one of the most common platforms used in metabolomics, offering thus a possibility to improve the resolution of metabolic flux maps in a variety of organisms.

Non-cyclic metabolic flux modes of guard cell TCA "cycle" in the light

Respiratory metabolism represents the major source of ATP in a wide range of organisms. In plants, beyond feeding the oxidative phosphorylation system (OxPHOS) with NADH and Succ, both glycolysis and the TCA cycle are important to provide carbon skeletons for the synthesis of amino acids, fatty acids, plant hormones and secondary

metabolites (Meyer *et al.*, 2019). In GCs, given their low photosynthetic capacity, which is associated to the low content of RubisCO and of chloroplast number (Willmer & Fricker, 1996), respiration seems to be the major source of the ATP needed to support stomatal opening in the light. This idea is additionally supported by the facts that, first, GCs have more mitochondria and higher respiration rate in comparison to MCs (Vani & Raghavendra, 1994; Araújo *et al.*, 2011c) and, second, that ATP treatment stimulates light-induced stomatal opening (Wang *et al.*, 2014a). Given the role of TCA cycle intermediates for stomatal movements regulation and the importance of ATP for sustaining guard cell plasma membrane ion activity (Flütsch *et al.*, 2020), the better understanding of the regulation of guard cell respiratory metabolism in the light becomes crucial to fully comprehend the mechanisms behind stomatal movement regulation, which will have direct and positive implications for metabolic modelling and plant metabolic engineer (Daloso *et al.*, 2017; Medeiros *et al.*, 2019).

The results obtained here reinforce the idea that the TCA cycle of GCs shows different non-cyclic flux modes, which run accordingly to the labelled substrate used. For instance, the ^{13}C derived from ^{13}C-Suc degradation was not incorporated into Mal, Fum or Succ. In contrast, a high ^{13}C enrichment was observed in Glu and Gln. This suggests an activation of the TCA cycle-C6 branch (from citrate to 2-OG) rather than of the C4 branch (from Mal to Succ) in GCs under light and ^{13}C-Suc. However, the data obtained for the rate of total ^{13}C-enrichment min^{-1} indicate that GCs under ^{13}C-HCO_3 have high ^{13}C incorporation into Fum, greater than that observed in MC-C3 under $^{13}CO_2$ (Figure 15). Given that the ^{13}C from ^{13}C-Suc was not detected in Mal, Fum and Succ and that an increase in M1 (*m/z* 118) was observed in both Glu and Gln over time (Figure 6), which refers to the carbon derived from PEPc activity, we hypothesize that labelled CO_2 is potentially being released from other metabolic reactions and subsequently incorporated into Glu/Gln through the C6 branch of the TCA cycle (Figure 20). The CO_2 released could be derived from reactions catalysed by different enzymes associated to the TCA cycle, such as malic enzymes (ME), PDH and IDH (Figure 19), in addition to the mitochondrial OGDH and the cytosolic oxidative pentose phosphate pathway. The results from Arabidopsis MCs from WT, *trxo1* mutant and *ntra ntrb* double mutant strongly suggests that PDH is an important source of labelled CO_2 for PEPc (discussed below in the section “The glycolytic fluxes toward Glu synthesis, via PEPc and PDH, seems to be negatively regulated by the mitochondrial TRX system in C3 mesophyll cells in the light”). However, plants have several metabolic reactions that are able to release

CO_2 (Sweetlove *et al.*, 2013). We thus cannot exactly conclude what are the exact sources of CO_2 labelled used by PEPc in GCs. Furthermore, the fate of Gln, to which extent and how it contributes to regulate stomatal opening are still open questions. Thus, the biological reason behind such ^{13}C incorporation into Gln is still unclear and thus require further experiments. Nonetheless, the activation of the TCA cycle-C4 branch is important for the synthesis of Mal and Fum, which are key regulators of stomatal movements, acting as respiratory substrate in the mitochondria, as K^+ counter-ion in the vacuole and/or as signalling compounds by activating chloride channels in the cytosol (Fernie & Martinoia, 2009; Araújo *et al.*, 2011b; De Angeli *et al.*, 2013; Eisenach & De Angeli, 2017; Hedrich & Geiger, 2017). Additionally, the synthesis of Succ is important to feed the complex II of the OxPHOS. Thus, on one hand, the C6 branch of guard cell TCA cycle seems to run to support the synthesis of Gln, whilst, on the other hand, the activation of the TCA cycle-C4 branch of GCs potentially acts as a mechanism to support stomatal opening by contributing to the osmotic balance of the cell and/or by stimulating ATP synthesis, which is then used by plasma membrane H^+-ATPases and the cell metabolism in general (Wang *et al.*, 2014a,b; Medeiros *et al.*, 2016, 2017).

Does guard cell TCA cycle occur in a non-cyclic, partially reverse mode?

It has been shown that the TCA cycle has several non-cyclic flux modes, that function accordingly to the organism, tissue and environmental condition (Sweetlove *et al.*, 2010; Steinhauser *et al.*, 2012). The C6 and C4 non-cyclic flux modes described on the previous section are commonly observed in leaves under light conditions (Tcherkez *et al.*, 2005, 2009; Gauthier *et al.*, 2010; Abadie *et al.*, 2017). However, other non-cyclic flux modes are found in microorganisms. For instance, certain bacteria, such as *Chlorobium*, show a completely reverse TCA cycle, which is an important pathway for CO_2 fixation in these organisms (Evans *et al.*, 1966; Buchanan & Arnon, 1990). In this context, it is interesting to note that in GCs under ^{13}C-HCO_3, Succ content significantly increased from 0 (dark) to 24 min after light imposition and decreased substantially afterwards (Figure 11). Similarly, the total ^{13}C enrichment in Succ *m/z* 247 significantly increased on the first 32 min upon light and then decreased towards 40 min (Figure 8). These results indicate that the carbon from ^{13}C-HCO_3 is used to the synthesis of Succ and that this metabolite is degraded over time after a brief exposure to light. Intriguingly, the total ^{13}C-enrichment in Glu *m/z* 246 showed a rapid increase from 32 to 40 min in GCs under ^{13}C-HCO_3 (Figure 10), in parallel to an increase in the intensity of both Glu M3 (*m/z* 249) and M4 (*m/z* 250) (Figure 6). Glu *m/z* 246 contains

four carbons of the Glu backbone, in which two carbons are derived from PDH activity and the other two from the TCA cycle (Figure 2). Although we did not detect Glu *m/z* 117-118 in this experiment, the results from ^{13}C-Suc showed an increase in Glu *m/z* 118 after 30 min in the light (Figure 6). Given that no ^{13}C enrichment in the C4 branch of the TCA cycle under ^{13}C-Suc was observed, these results indicate that the carbon from PEPc is directed to Glu via TCA cycle-C6 branch (Figure 7). Thus, Glu is fully labelled in GCs during dark-to-light transition by a combination of ^{13}C derived from PEPc, glycolysis, which enters the TCA cycle through PDH, and the TCA cycle. Assuming that the TCA cycle does not work in a cyclic mode in the light, a reasonable hypothesis to explain fully labelled Glu in GCs under ^{13}C-HCO_3 is an association of Succ degradation and Glu synthesis. In this scenario, the TCA cycle would run in a non-cyclic, partially reverse mode. In terms of functionality for guard cell metabolism, this partial reverse mode would contribute to the overall CO_2 fixation of the cell, given that a molecule of CO_2 would be fixed from succinyl CoA to 2-OG (Figure 20). However, the results observed here *per se* do not allow us to conclude that GCs TCA cycle shows a non-cyclic, partially reverse mode. Fully labelled Glu *m/z* 246 could also be interpreted by a combination of labelled carbons entering the TCA cycle through the activity of PDH, pyruvate carboxylase (PC) and PEPc using fully labelled pyruvate and PEP and producing fully labelled OAA and AcCoA (Figure 17). In this scenario, the reduction observed on Succ labelling and content could be interpreted as a potential consumption of this metabolite by OxPHOS. Further ^{13}C-feeding experiments and enzymatic characterization of guard cell TCA cycle enzymes are thus necessary to test the hypothesis that guard cell TCA cycle runs in a non-cyclic, partially reverse mode. Our study contributes to emphasize that the TCA cycle display different patterns of regulation amongst cell types and that the identification of distinct TCA cycle flux modes and their regulatory mechanisms is a challenge to overcome.

Similarities and differences between guard cells and sink-C3 mesophyll cells.

Recently, sink and source Arabidopsis leaves were evaluated under ^{13}C-Suc, revealing substantial differences in their metabolism (Dethloff *et al.*, 2017). We took advantage of this well-performed work to check the similarities of the ^{13}C distribution observed throughout the TCA cycle between GCs with and sink and source MC-C3. However, given that the labelling time used in this study differs substantially from those of GCs, we did not compare them statistically. We used this qualitative comparison with the aim to identify the typical labelling

patterns derived from Suc degradation in sink and source MC-C3 and to compare them to the pattern observed in GCs. GCs are known to have several characteristics that resemble sink MCs (Daloso *et al.*, 2016). In close agreement with this idea, we found that the distribution pattern of the carbon derived from ^{13}C-Suc in GCs is more similar to sink rather than to source MCs. For instance, sink MC-C3 showed 3-fold higher total ^{13}C-enrichment in Gln than source MC-C3 (Figure 16). Similarly, GCs had higher total ^{13}C-enrichment min^{-1} in Gln from ^{13}C-Suc, when compared to MC-C3 or MC-C4 under $^{13}CO_2$ (Figure 15). However, sink MC-C3 showed higher total ^{13}C-enrichment in Mal than source MC-C3 (Figure 16), and this was not observed in GCs compared to MC-C3 under $^{13}CO_2$ (Figure 15). This is probably due to the fact that MC-C3 under $^{13}CO_2$ showed higher ^{13}C incorporation into Mal derived from PEPc activity, as evidenced by the higher values of total ^{13}C-enrichment min^{-1} on the Mal *m/z* 117 (Figure 14). However, no difference was observed in the total ^{13}C-enrichment min^{-1} in Mal *m/z* 233 between GCs under ^{13}C-HCO_3 and MC-C3 under $^{13}CO_2$, indicating that labelling of the carbons 2 and 3 of Mal backbone do not differ or is higher in GCs than in MC-C3. Furthermore, the analysis made by Dethloff and collaborators (2017) of the fragment Mal *m/z* 245, which contains the four carbons of the Mal backbone, showed that only three carbons have been labelled in sink MC-C3 after 240 min under ^{13}C-Suc (Figure 16). This indicates that one carbon is not labelled under this condition, which could represent the carbon derived from PEPc activity. However, the lack of data from Mal *m/z* 117-118 for sink MC-C3 under ^{13}C-Suc hampers us to conclude that there was no incorporation of ^{13}C from Suc into the carbon 4 of Mal.

A remarkable difference found between GCs and MCs was the ^{13}C incorporation into Ala. Whilst sink and source MC-C3 had no difference in the content or in the total ^{13}C-enrichment in Ala (Figure 16), GCs under ^{13}C-Suc had higher total ^{13}C-enrichment min^{-1} in Pyr and much lower total ^{13}C-enrichment min^{-1} in Ala, as compared to MC-C3 under $^{13}CO_2$ (Figure 9). Furthermore, whilst Pyr content reduced substantially over time, Ala content did not change in GCs under ^{13}C-Suc (Figure 12). This indicates that, during dark-to-light transition, glycolysis pathway has a minor importance in providing carbon for the synthesis of Ala in GCs (Figure 7). Instead, we observed a high incorporation of carbon derived from Pyr into Glu/Gln in GCs, as evidenced by the progressive increase in Glu M2 (*m/z* 248) over time. Taken together, these results indicate that PDH offers no, or at least lesser, restriction to the entrance of carbon into the TCA cycle in GCs upon light, when compared to MC-C3 under $^{13}CO_2$ (discussed below in the topic “The glycolytic fluxes toward Glu synthesis, via PEPc

and PDH, seems to be negatively regulated by the mitochondrial TRX system in C3 mesophyll cells in the light**"**).

Another notable difference observed in GCs, when compared to MCs, is the number of ^{13}C incorporated into Glu and Gln. Whilst in GCs Glu *m/z* 246 and, in particular, Gln *m/z* 245 clearly had the incorporation of four labelled carbons after 60 min under ^{13}C-Suc, only two labelled carbons were incorporated into Glu in sink MC-C3 under ^{13}C-Suc (Figure 16) and in MC-C3 under $^{13}CO_2$ (Figure 7). Furthermore, no ^{13}C-enrichment in Gln *m/z* 245 was observed in MC-C3 and MC-C4 under $^{13}CO_2$ (Figure 7). These results evidence that GCs have a higher metabolic flux of carbon toward Glu and Gln in the light, with preference for Gln synthesis. It is important to highlight, however, that non-fully labelled Glu observed in sink MC-C3 could be a result of an isotope dilution due to the incorporation of previous stored ^{12}C in the form of citrate (Cheung *et al.*, 2014; Abadie *et al.*, 2017; Dethloff *et al.*, 2017). Furthermore, sink MC-C3 showed higher maltose content with no ^{13}C-enrichment from ^{13}C-Suc, suggesting that the degradation of previous stored starch in sink MC-C3 would also contribute to dilute the ^{13}C incorporation, if we consider that carbons derived from starch are directed to TCA and Glu synthesis. Interestingly, GCs also show starch degradation in the first hour of light (Horrer *et al.*, 2016; Antunes *et al.*, 2017), as a mechanism to speed up light-induced stomatal opening (Flütsch *et al.*, 2020). Taken together, these results evidence that GCs have intrinsic metabolic characteristics of sink cells in terms of a high allocation of carbon to the synthesis of Gln and starch degradation in the light, but with a particular difference in the carbon contributions from glycolysis pathway and the TCA cycle to Gln synthesis.

Role of PEPc in providing carbon for the TCA cycle and Glu/Gln synthesis

The anaplerotic CO_2 fixation mediated by PEPc involves the incorporation of HCO_3 into OAA using PEP as substrate with the production of Pi (Melzer & O'Leary, 1987; O'Leary *et al.*, 2011). Whilst the role of PEPc for CO_2 assimilation in C4 cells is well-documented, the importance of anaplerotic CO_2 fixation mediated by PEPc have often been neglected in C3 plants and not taken into account in gas exchange measurements. The PEPc activity in C3 plants have been attributed to generate OAA that is further used for the synthesis of metabolites associated to the TCA cycle (Abadie and Tcherkez, 2019). Indeed, a remarkable study showed that Arabidopsis plants lacking PEPc 1 and 2 have severe reduced growth, which was associated to a disruption in the accumulation of nitrate, Mal, citrate and

of diverse amino acids, including Asp and Glu (Shi *et al.*, 2015). Given the instability of OAA, an alternative to analyse PEPc activity is by measuring the incorporation of the ^{13}C derived from PEPc activity into Asp or Mal, which are direct products of OAA degradation catalysed by aspartate aminotransferase (AspAT) and malate dehydrogenase (MDH), respectively (Abadie & Tcherkez, 2019). Here we identified and used the fragment *m/z* 117 of Mal that contains the ^{13}C fixed by PEPc into the carbon-4 of OAA and subsequently transferred to the carbon-4 of Mal (Figure 3). We also analysed the ^{13}C-enrichment in the fragment *m/z* 233 of Mal that contains the carbons 2, 3 and 4 of the Mal backbones (Figure 14).

As expected, our results showed that the total ^{13}C-enrichment in Mal *m/z* 117 is higher in MC-C4 than MC-C3, evidencing the feasibility of the positional isotope labelling approach. Surprisingly, however, MC-C3 under $^{13}CO_2$ had higher both total ^{13}C-enrichment and total ^{13}C-enrichment min^{-1} in Mal *m/z* 117 than GCs under ^{13}C-HCO_3, although the total ^{13}C-enrichment min^{-1} in malate *m/z* 233 was slightly higher in GCs than MC-C3 (Figure 14). Considering that the ^{13}C enrichment in Mal *m/z* 233 also includes the intensity found in the carbon-4, which was higher in MC-C3, this suggests that the incorporation of ^{13}C into the carbons 2 and 3 of the Mal backbone is higher in GCs. In this scenario, GCs would have higher activity of pyruvate carboxylase (PC), that converts Pyr into OAA, which is then converted to Mal by MDH. In addition, it is important to highlight that great part of the carbon assimilated by PEPc is used for Glu/Gln synthesis through the C6 branch, as evidenced by, first, the increased *m/z* 118 in Glu (Figure 6) and especially in Gln and, second, by the lack of ^{13}C-enrichment in Mal, Fum and Succ under ^{13}C-Suc (Figure 15). Thus, we cannot currently conclude that GCs have lower PEPc activity. In fact, previous metabolic coupled to modelling results suggest that GCs have higher anaplerotic CO_2 assimilation than MCs (Robaina-estevez et al 2017). Further ^{13}C-feeding experiments working with both MCs and GCs under the same environmental conditions and labelled substrate, with similar harvesting time points may answer the question of whether *in vivo* PEPc activity is higher in MCs than in GCs of C3 plants. Given that PEPc is key for metabolic engineering aiming to transform C3 into C4 plants, understanding the regulation and the *in vivo* capacity of PEPc in different cell types and species assumes thus a paramount importance.

The glycolytic fluxes toward Glu synthesis, via PEPc and PDH, seems to be negatively regulated by the mitochondrial TRX system in C3 mesophyll cells in the light

PDH is a complex composed of three subunits (E1, E2 and E3) that ultimately converts Pyr into AcCoA in plastids or mitochondria (Guan *et al.*, 1995; Millar *et al.*, 1998). The mitochondrial PDH represents an important reaction that provides carbon to the TCA cycle. However, PDH is inactivated by reversible phosphorylation of the two Serine residues of the E1 α subunit under light condition (Thelen *et al.*, 2000; Tovar-Méndez *et al.*, 2003). The phosphorylation state of PDH complex relies on PDH kinase (PDK) and phosphopyruvate dehydrogenase phosphatase (PDP) that, in turn, are activated by NH_3 and ATP and inhibited by pyruvate and ADP (McDonald & Vanlerberghe, 2018). Thus, as the levels of ATP, NADH and NH_3 coming from photorespiration increase, PDH is inactivated throughout the day (Gemel and Randall, 1992; McDonald & Vanlerberghe, 2018). Under light condition, both AlaAT and AspAT are more abundant (Lee *et al.*, 2008), what may represent a bypass of the TCA cycle, given that PDH is less active. Interestingly, our meta-analysis showed that the total ^{13}C- enrichment in Ala is much higher in MC-C3 than in GCs (Figure 15), suggesting that the light inhibition of PDH in MCs forces the glycolytic fluxes to bypass the TCA cycle through AlaAT. It is noteworthy that AlaAT does not only play a role in amino acid metabolism by producing Ala, but it also catalyses the formation of 2-OG from Glu through the transamination of Pyr and OAA, that may be used to fuel both the later steps of TCA cycle and the assimilation of N outside the mitochondria (Miyashita *et al.*, 2007; Lee *et al.*, 2008, Xu *et al.*, 2017). This represents an alternative route to feed the TCA cycle in the light, when PDH is inhibited, as already demonstrated in *Lotus japonicus* plants under hypoxia (Rocha *et al.*, 2010). Here, MC-C4 had an extremely fast ^{13}C-enrichment in Pyr and Ala, as evidenced by the linear increase observed in Pyr M3 (*m/z* 177) and Ala M2 (*m/z* 118) (Figure 5). This can be explained by a combination of labelled carbon coming from glycolysis (after CO_2 fixation by RubisCO) and from the activity of ME, which converts Mal, produced from PEPc activity, into Pyr (Figure 19). Interestingly, GCs also showed an increased Pyr M3 (*m/z* 177) under ^{13}C-Suc over time, leading to statistically higher total ^{13}C-enrichment min^{-1} than MC-C3 under $^{13}CO_2$ (Figure 15). This result suggests that the glycolytic fluxes are higher in GCs than MC-C3. Indeed, it has been shown that the level of hexose phosphate decreases while fructose-1,6-bisphosphate increases 6-fold after dark-to-light transition in GCs (Hedrich *et al.*, 1985). Furthermore, plants lacking the glycolytic enzyme phosphoglycerate mutase have compromised blue light-induced stomatal opening (Zhao &

Assmann, 2011), evidencing the importance of glycolysis activation for the regulation of stomatal opening.

A recent modelling study suggests that mitochondrial respiration must have substantial ATP synthesis to support the cytosolic ATP demand in the light, as the transport of ATP synthesized in the chloroplast to the cytosol is limited by plastidial ATP export shuttles (Shameer *et al.*, 2019). Thus, plants may have alternative pathways and regulatory mechanisms to overcome the limitation imposed by the light-inhibition of mitochondrial PDH and the light inhibition of succinate dehydrogenase and fumarase (Daloso *et al.*, 2015b; Eprintsev *et al.*, 2016a,b; Eprintsev *et al.*, 2018), which together restricts the fluxes throughout the TCA cycle and reduce the respiration rate in the light (Gong *et al.*, 2018; Tcherkez *et al.*, 2012). In this vein, in order to obtain more insights on how PDH is regulated, we also evaluated data from a study that have used three different labelled substrates (^{13}C-Glc, ^{13}C-Pyr and ^{13}C-Mal) and three Arabidopsis genotypes (WT, *trxo1* and *ntra ntrb*). This analysis revealed a higher total ^{13}C-enrichment min^{-1} in Pyr from ^{13}C-Glc than from ^{13}C-Mal (Figure 17), indicating that both glycolysis and the ME contribute to the ^{13}C incorporation into Pyr in the light (Figure 19), although this contribution seems much lower than that observed in MC-C4 (Figure 15). Mal and Fum were labelled at the same rate by both ^{13}C-Glc and ^{13}C-Pyr (Figure 17), further confirming that glycolytic carbons are also directed to the C4 branch of the TCA cycle and highlights a role of PEPc and PC for Mal and Fum synthesis in MC-C3 in the light (Figure 17).

Our meta-analysis suggests that the light inhibition of the mitochondrial PDH is an important step that modulates the fluxes from PEPc and the TCA cycle toward Glu synthesis. This idea is supported by the results in which Glu *m/z* 117 was only labelled by ^{13}C-Pyr and Glu *m/z* 246 was labelled by all substrates, but in a greater extent under ^{13}C-Pyr (Figure 17), which may have intensified PDH activity by increasing substrate availability. Given that Glu *m/z* 117 contains the carbon 1 of the Glu backbone, which is derived from PEPc fixation, it seems likely that PEPc frequently use the CO_2 released by PDH and/or IDH (Figure 19). Additionally, given that ^{13}C-enrichment in Glu *m/z* 117 under ^{13}C-Glc was only observed in *trxo1* and *ntra ntrb* mutants, this suggests that the mitochondrial NTR/TRX system is a negative regulator of this pathway *in vivo*. In this scenario, the lack of TRX *o1* or both NTRA/NTRB would make PDH and/or IDH more active, increasing therefore the rate of labelled CO_2 released, which is then transported out of mitochondria and fixed by PEPc (Figure 19). However, mitochondrial IDH is known to be activated by TRXs *in vitro* (Yoshida

& Hisabori, 2014) and the lack of *trxo1* did not change the activity of IDH (Daloso *et al.*, 2015b). By contrast, it has been recently shown that both TRX *o1* and TRX *h2* (another mitochondrial TRX) inhibit the activity of the mitochondrial dihydrolipoamide dehydrogenase (mtLPD) *in vitro*, which correspond to the E3 subunit of PDH (Reinholdt *et al.*, 2019b; Fonseca-Pereira *et al.*, 2020). Thus, the lack of TRX *o1* or NTRA plus NTRB may had positive consequences for PDH activity, and not for IDH. Further evidence supporting the idea that PDH is an important source of CO_2 for PEPc comes from a ^{14}C-feeding experiment in which the rate of CO_2 evolved from the TCA cycle associated enzymes (mainly PDH) is higher in the *trxo1* mutant (Florez-Sarasa *et al.*, 2019). However, it is important to note that the lack of TRX *o1* substantially alter the activity of several TCA cycle enzymes (Daloso *et al.*, 2015b) and that the mtLPD is also included in the glycine decarboxylase complex, which is an important source of NADH and CO_2 in the mitochondrion (Timm *et al.*, 2015; Fonseca-Pereira *et al.*, 2020;). Furthermore, NAD-ME could also represent an important source of CO_2 under this condition (Figure 19). Furthermore, PDH might represent an important source of CO^2 released that is used by PEPc. Taken together, these results contribute to explain the higher fluxes throughout the TCA cycle in the light (Daloso *et al.*, 2015b; Florez-Sarasa *et al.*, 2019) and the higher ^{13}C incorporation observed in the carbon 1 of Glu in both *trxo1* and *ntra ntrb* mutants under ^{13}C-Glc. This strengthen the idea that redox regulation mediated by TRXs is an important control point that modulates metabolic fluxes throughout the TCA cycle in the light.

Concluding remarks

Here we present an ^{13}C-positional isotope labelling approach to study metabolic fluxes, based on the development of metabolite fragmentation maps and on *in silico* simulations of metabolite fragmentation. This approach enables the investigation of the incorporation of the carbon fixed by PEPc into Mal, Glu and Gln as well as to distinguish the differential contributions of glycolysis and the TCA cycle from that of PEPc-CO_2 fixation to the synthesis of Glu and Gln. In addition, our ^{13}C-positional isotope labelling approach showed to be an effective tool to be potentially applied to any organism on the study of metabolic fluxes and to be used as a feasible alternative to be further adapted to measure PEPc activity *in vivo* through the use of GC-EI-MS data.

The results of our meta-analysis using this ^{13}C-positional isotope labelling approach suggest that GCs have particular metabolic flux modes throughout the TCA cycle and

associated pathways, with certain similarities with sink MC-C3 and several discrepancies to source MC-C3 (Figure 20). Notably, although MC-C4 and MC-C3 seem to have higher PEPc activity than GCs, the use of the carbon incorporated into OAA to the synthesis of citrate, using AcCoA from PDH activity, seems to be higher in GCs than in all other cell types analysed here. Consequently, this increases the fluxes from OAA to Gln synthesis through the C6 branch of the TCA cycle in GCs (Figure 20), which may have led to an underestimation of the rate of ^{13}C assimilation mediated by PEPc in GCs. In addition, the TCA cycle-C4 branch of GCs resembles that observed in sink leaves, but with a particular ^{13}C-enrichment and accumulation of Fum in GCs. Finally, our work provides further insights into the redox regulation mediated by the mitochondrial TRX system over the TCA cycle and associated pathways in mesophyll cells in the light, extending the regulatory control of this system to Glu synthesis. In this context, our meta-analysis indicates that the light-dependent inhibition of PDH severely restrict the fluxes to Glu and enhances the glycolytic fluxes to bypass the TCA cycle toward Ala. Given that GCs did not show restrictions to the glycolytic fluxes toward Glu and Gln, this suggests that guard cell TCA cycle enzymes and especially PDH are differentially regulated in the light, as compared to MCs.

Acknowledgments

This work was supported by funding from National Council for the Improvement of Higher Education (CAPES) and National Council for Scientific and Technological Development (CNPq). Scholarship was granted by CAPES. I thank the authors that kindly provided their data of already published works.

References

Abadie C, Tcherkez G. 2019. In vivo phosphoenolpyruvate carboxylase activity is controlled by CO_2 and O_2 mole fractions and represents a major flux at high photorespiration rates. *New Phytologist* **221**: 1843-1852.

Abadie C, Lothier J, Boex-Fontvieille E, Carroll A, Tcherkez G. **2017**. Direct assessment of the metabolic origin of carbon atoms in glutamate from illuminated leaves using ^{13}C-NMR. *New Phytologist* **216**: 1079–1089.

Allen DK, Ohlrogge JB, Shachar-Hill Y. **2009**. The role of light in soybean seed filling metabolism. *The Plant Journal* **58**: 220–234.

Alonso AP, Goffman FD, Ohlrogge JB, Shachar-Hill Y. **2007**. Carbon conversion efficiency and central metabolic fluxes in developing sunflower (*Helianthus annuus* L.) embryos. *Plant Journal* **52**: 296–308.

De Angeli A, Zhang J, Meyer S, Martinoia E. **2013**. AtALMT9 is a malate-activated vacuolar chloride channel required for stomatal opening in Arabidopsis. *Nature Communications* **4**: 1804–1810.

Antoniewicz MR. **2013**. Tandem mass spectrometry for measuring stable-isotope labeling. *Current Opinion in Biotechnology* **24**: 48–53.

A**ntoniewicz MR, Kelleher JK, Stephanopoulos G. 2007**. Accurate assessment of amino acid mass isotopomer distributions for metabolic flux analysis. *Analytical chemistry* **79:** 7554–7559.

Antunes WC, Daloso DM, Pinheiro DP, Williams TCR, Loureiro ME. **2017**. Guard cell-specific down-regulation of the sucrose transporter SUT1 leads to improved water use efficiency and reveals the interplay between carbohydrate metabolism and K^+ accumulation in the regulation of stomatal opening. *Environmental and Experimental Botany* **135**: 73–85.

Araújo WL, Fernie AR, Nunes-Nesi A. **2011a**. Control of stomatal aperture: A renaissance of the old guard. *Plant Signaling and Behavior* **6**: 1305–1311.

Araújo WL, Nunes-Nesi A, Fernie AR. **2011b**. Fumarate: Multiple functions of a simple metabolite. *Phytochemistry* **72**: 838–843.

Araújo WL, Trofimova L, Mkrtchyan G, Steinhauser D, Krall L, Graf A, Fernie AR, Bunik VI. **2013**. On the role of the mitochondrial 2-oxoglutarate dehydrogenase complex in

amino acid metabolism. *Amino Acids* **44**: 683–700.

Araújo WL, Nunes-Nesi A, Osorio S, Usadel B, Fuentes D, Nagy R, Balbo I, Lehmann M, Studart-Witkowski C, Tohge T, *et al.* 2011c. Antisense inhibition of the iron-sulphur subunit of succinate dehydrogenase enhances photosynthesis and growth in tomato via an organic acid–mediated effect on stomatal aperture. *The Plant Cell* **23**: 600–627.

Araujo WL, Nunes-Nesi A, Trenkamp S, Bunik VI, Fernie AR. **2008**. Inhibition of 2-Oxoglutarate dehydrogenase in potato tuber suggests the enzyme is limiting for respiration and confirms its importance in nitrogen assimilation. *Plant Physiology* **148**: 1782–1796.

Balmer Y, Vensel WH, Tanaka CK, Hurkman WJ, Gelhaye E, Rouhier N, Jacquot J-P, Manieri W, Schurmann P, Droux M, *et al.* 2004. Thioredoxin links redox to the regulation of fundamental processes of plant mitochondria. *Proceedings of the National Academy of Sciences* **101**: 2642–2647.

Beevers H. **1961**. *Respiratory Metabolism in Plants*. New York: Harper and Row.

Buchanan BB, Arnon DI. **1990**. A reverse KREBS cycle in photosynthesis: consensus at last. *Photosynthesis Research* **24**: 47–53.

Buchanan BB. **2016**. The carbon (formerly dark) reactions of photosynthesis. *Photosynthesis Research* **128**: 215–217.

Buchanan BB. **2017**. The path to thioredoxin and redox regulation beyond chloroplasts. *Plant and Cell Physiology* **58**: 1826–1832.

Cheung CYM, Poolman MG, Fell DA, Ratcliffe RG, Sweetlove LJ. **2014**. A diel flux balance model captures interactions between light and dark metabolism during day-night cycles in C3 and crassulacean acid metabolism leaves. *Plant Physiology* **165**: 917–929.

Daloso DM, Antunes WC, Pinheiro DP, Waquim JP, Araújo WL, Loureiro ME, Ferine AR, Williams TC. 2015a. Tobacco guard cells fix CO_2 by both Rubisco and PEP case while sucrose acts as a substrate during light-induced stomatal opening. *Plant, cell & environment* **38**: 2353-2371.

Daloso DM, Müller K, Obata T, Florian A, Tohge T, Bottcher A, Riondet C, Bariat L, Carrari F, Nunes-Nesi A, Buchanan BB, Reichheld JP, Araújo WL, Fernie AR. 2015b. Thioredoxin, a master regulator of the tricarboxylic acid cycle in plant mitochondria. *Proceedings of the National Academy of Sciences* **112**: E1392-E1400.

Daloso DM, dos Anjos L, Fernie AR. **2016**. Roles of sucrose in guard cell regulation. *New Phytologist* **211**: 809–818.

Daloso DM, Medeiros DB, dos Anjos L, Yoshida T, Araújo WL, Fernie AR. **2017**. Metabolism within the specialized guard cells of plants. *New Phytologist* **216**: 1018–1033.

Dejongh DC, Radford T, Hribar JD, Hanessian S, Bieber M, Dawson G. **1969**. Analysis of trimethylsilyl derivatives of carbohydrates by gas chromatography and mass spectrometry. J*ournal of the American Chemical Society* **91**: 1728–1740.

Dethloff F, Orf I, Kopka J. **2017**. Rapid in situ13C tracing of sucrose utilization in Arabidopsis sink and source leaves. *Plant Methods* **13**: 1–19.

Eprintsev AT, Fedorin DN, Cherkasskikh M V., Igamberdiev AU. 2018. Expression of succinate dehydrogenase and fumarase genes in maize leaves is mediated by cryptochrome. *Journal of Plant Physiology* **221**: 81–84.

Eprintsev AT, Fedorin DN, Karabutova LA, Igamberdiev AU. 2016a. Expression of genes encoding subunits A and B of succinate dehydrogenase in germinating maize seeds is regulated by methylation of their promoters. *Journal of Plant Physiology* **205**: 33–40.

Eprintsev AT, Fedorin DN, Sazonova O V., Igamberdiev AU. 2016b. Light inhibition of fumarase in Arabidopsis leaves is phytochrome A-dependent and mediated by calcium. *Plant Physiology and Biochemistry* **102**: 161–166.

Eisenach C, De Angeli A. **2017**. Ion transport at the vacuole during stomatal movements. *Plant Physiology* **174**: 520–530.

Evans MC, Buchanan BB, Arnon DI. **1966**. A new ferredoxin-dependent carbon reduction cycle in a photosynthetic bacterium. *Proceedings of the National Academy of Sciences of the United States of America* **55**: 928–934.

Fernie AR, Martinoia E. **2009**. Malate. Jack of all trades or master of a few? *Phytochemistry* **70**: 828–832.

Fernie AR, Stitt M. **2012**. On the discordance of metabolomics with proteomics and transcriptomics: coping with increasing complexity in logic, chemistry, and network interactions scientific correspondence. *Plant Physiology* **158**: 1139–1145.

Fernie AR, Zhang Y, Sweetlove LJ. **2018**. Passing the baton : substrate channelling in

respiratory metabolism. *Research* **2018**: 1–16.

Finkemeier I, Laxa M, Miguet L, Howden AJM, Sweetlove LJ. **2011**. Proteins of diverse function and subcellular location are lysine acetylated in Arabidopsis. *Plant Physiology* **155**: 1779–1790.

Florez-Sarasa I, Obata T, Del-Saz NF, Reichheld J-P, Meyer EH, Rodriguez-Concepcion M, Ribas-Carbo M, Fernie AR. 2019. The lack of mitochondrial thioredoxin TRXo1 affects in vivo alternative oxidase activity and carbon metabolism under different light conditions. *Plant & Cell Physiology* **60**: 2369-2381.

Flütsch S, Wang Y, Takemiya A, Vialet-Chabrand S, Klajchova M, Nigro A, Hills A, Lawson T, Blatt MR, Santelia D. **2020**. Guard cell starch degradation yields glucose for rapid stomatal opening in Arabidopsis. *Pant Cell* **32**: 2325–2344.

Fonseca-Pereira P, Souza PVL, Hou LY, Schwab S, Geigenberger P, Nunes-Nesi A, Timm S, Fernie AR, Thormählen I, Araújo WL, Daloso DM. 2020. Thioredoxin h2 contributes to the redox regulation of mitochondrial photorespiratory metabolism. *Plant, Cell & Environment* **43**: 188–208.

Gauthier PPG, Bligny R, Gout E, Mahé A, Nogués S, Hodges M, Tcherkez GGB. **2010**. In folio isotopic tracing demonstrates that nitrogen assimilation into glutamate is mostly independent from current CO_2 assimilation in illuminated leaves of Brassica napus. *New Phytologist* **185**: 988–999.

Gong XY, Tcherkez G, Wenig J, Schäufele R, Schnyder H. 2018. Determination of leaf respiration in the light: comparison between an isotopic disequilibrium method and the Laisk method. *New Phytologist* **218**: 1371–1382.

Gotow K, Taylor S, Zeiger E. **1988**. Photosynthetic carbon fixation in guard cell protoplasts of *Vicia faba* L. *Plant Physiol* **86**: 700–705.

Guan Y, Rawsthorne S, Scofield G, Shaw P, Doonan J. 1995.Cloning and characterization of a dihydrolipoamide acetyltransferase (E2) subunit of the pyruvate dehydrogenase complex from Arabidopsis thaliana. *J Biol Chem* **270**: 5412–5417.

Hanning I, Held HW. 1993. On the function of mitochondrial metabolism during photosynthesis in spinach (*Spinacia oleracea* L.) leaves (partitioning between respiration and export of redox equivalents and precursors for nitrate assimilation products). *Plant Physiology*

103: 1147-1154.

Hedrich R, Geiger D. **2017**. Biology of SLAC1-type anion channels - from nutrient uptake to stomatal closure. *New Phytologist* **216**: 46–61.

Hedrich R, Raschke K, Stitt M. **1985**. A role for fructose 2,6-bisphosphate in regulating carbohydrate metabolism in guard cells. *Plant physiology* **79**: 977–982.

Heise R, Arrivault S, Szecowka M, Tohge T, Nunes-Nesi A, Stitt M, Nikoloski Z, Fernie AR. **2014**. Flux profiling of photosynthetic carbon metabolism in intact plants. *Nature Protocols* **9**: 1803–1824.

Horrer D, Flütsch S, Pazmino D, Matthews JSA, Thalmann M, Nigro A, Leonhardt N, Lawson T, Santelia D. **2016**. Blue light induces a distinct starch degradation pathway in guard cells for stomatal opening. *Current Biology* **26**: 362–370.

Huege J, Sulpice R, Gibon Y, Lisec J, Koehl K, Kopka J. 2007. GC-EI-TOF-MS analysis of in vivo carbon-partitioning into soluble metabolite pools of higher plants by monitoring isotope dilution after $^{13}CO_2$ labelling. *Phytochemistry* **68**: 2258-2272.

Kim HK, Choi YH, Verpoorte R. **2010**. NMR-based metabolomic analysis of plants. *Nature Protocols* **5**: 536–549.

Krebs HA, Johnson WA. **1937**. Metabolism of ketonic acids in animal tissues. *Biochemical Journal* **31**: 645–660.

Lawson T, Oxborough K, Morison JIL, Baker NR. **2003**. The responses of guard and mesophyll cell photosynthesis to CO_2, O_2, light, and water stress in a range of species are similar. *Journal of Experimental Botany* **54**: 1743–1752.

Lawson T, Vialet-Chabrand S. **2018**. Speedy stomata, photosynthesis and plant water use efficiency. *New Phytologist* **221**: 93–98.

Leimer KR, Rice RH, Gehrke CW. 1977. Complete mass spectra of the per-trimethylsilylated amino acids. *Journal of Chromatography A* **141**: 355-375.

Lima VF, Medeiros DB, Dos Anjos L, Gago J, Fernie AR, Daloso DM. **2018a**. Toward multifaceted roles of sucrose in the regulation of stomatal movement. *Plant Signaling & Behavior* **13**: 1–8.

Lima VF, de Souza LP, Williams TCR, Fernie AR, Daloso DM. **2018b**. Gas

chromatography–mass spectrometry-based ^{13}C-labeling studies in plant metabolomics. *Plant Metabolomics* **1778**: 47–58.

Lee, C. P., Eubel, H., O'Toole, N., & Millar, A. H. 2008. Heterogeneity of the mitochondrial proteome for photosynthetic and non-photosynthetic Arabidopsis metabolism. *Molecular & Cellular Proteomics* **7**: 1297-1316.

Lisec J, Schauer N, Kopka J, Willmitzer L, Fernie AR. 2006. Gas chromatography mass spectrometry–based metabolite profiling in plants. *Nature protocols* **1**, 387.

McDonald AE, Vanlerberghe GC. 2018. The organization and control of plant mitochondrial metabolism. *Annual Plant Reviews online* **2018**: 290-324.

Medeiros DB, Barros KA, Barros JAS, Omena-Garcia RP, Arrivault S, Sanglard LMVP, Detmann KC, Silva WB, Daloso DM, DaMatta FM, Nunes-Nesi A, Fernie AR, Araújo WL. 2017. Impaired malate and fumarate accumulation due to the mutation of the tonoplast dicarboxylate transporter has little effects on stomatal behavior. *Plant Physiology* **175**: 1068–1081.

Medeiros DB, da Luz LM, de Oliveira HO, Araújo WL, Daloso DM, Fernie AR. **2019**. Metabolomics for understanding stomatal movements. *Theoretical and Experimental Plant Physiology* **9**: 91–102.

Medeiros DB, Martins SCV, Cavalcanti JHF, Daloso DM, Martinoia E, Nunes-Nesi A, DaMatta FM, Fernie AR, Araújo WL. **2016**. Enhanced photosynthesis and growth in atquac1 knockout mutants are due to altered organic acid accumulation and an increase in both stomatal and mesophyll conductance. *Plant Physiology* **170**: 86–101.

Medeiros DB, Perez Souza L, Antunes WC, Araújo WL, Daloso DM, Fernie AR. **2018**. Sucrose breakdown within guard cells provides substrates for glycolysis and glutamine biosynthesis during light-induced stomatal opening. *The Plant Journal* **94**: 583–594.

Melzer E, O'Leary MH. **1987**. Anapleurotic CO_2 Fixation by Phosphoenolpyruvate Carboxylase in C3 Plants. *Plant Physiology* **84**: 58–60.

Meyer EH, Welchen E, Carrie C. **2019**. Assembly of the complexes of the oxidative phosphorylation system in land plant mitochondria. *Annual Review of Plant Biology* **70**: 23–50.

Millar AH, Knorpp C, Leaver CJ, Hill SA. 1998. Plant mitochondrial pyruvate

dehydrogenase complex: purification and identification of catalytic components in potato. *Biochemical Journal* **334:** 571-576.

Miyashita Y, Dolferus R, Ismond KP, Good AG. 2007. Alanine aminotransferase catalyses the breakdown of alanine after hypoxia in Arabidopsis thaliana. *The Plant Journal* **49**: 1108-1121.

Møller IM, Rasmusson AG. **1998**. The role of NADP in the mitochondrial matrix. *Trends in Plant Science* **3**: 21–27.

Nietzel T, Mostertz J, Hochgräfe F, Schwarzländer M. **2017**. Redox regulation of mitochondrial proteins and proteomes by cysteine thiol switches. *Mitochondrion* **33**: 72–83.

Nunes-Nesi A, Araújo WL, Obata T, Fernie AR. **2013**. Regulation of the mitochondrial tricarboxylic acid cycle. *Current Opinion in Plant Biology* **16**: 335–343.

Obata T, Florian A, Timm S, Bauwe H, Fernie AR. **2016**. On the metabolic interactions of (photo)respiration. *Journal of Experimental Botany* **67**: 3003–3014.

Okahashi N, Kawana S, Iida J, Shimizu H, Matsuda F. 2019. Fragmentation of dicarboxylic and tricarboxylic acids in the krebs cycle using GC-EI-MS and GC-EI-MS/MS. *Mass Spectrometry **8**:* A0073.

O'Leary B, Park J, Plaxton WC. **2011**. The remarkable diversity of plant PEPC (phosphoenolpyruvate carboxylase): recent insights into the physiological functions and post-translational controls of non-photosynthetic PEPCs. *Biochemical Journal* **436**: 15–34.

Petersson G. 1972. Mass spectrometry of hydroxy dicarboxylic acids as trimethylsilyl derivatives. Rearrangement fragmentations. *Organic Mass Spectrometry* **6:** 565-576.

Ratcliffe RG, Shachar-Hill Y. **2006**. Measuring multiple fluxes through plant metabolic networks. *The Plant Journal* **45**: 490–511.

Reinholdt O, Bauwe H, Hagemann M, Timm S. **2019a**. Redox-regulation of mitochondrial metabolism through thioredoxin o1 facilitates light induction of photosynthesis. *Plant Signaling and Behavior* **14**: 1674607.

Reinholdt O, Schwab S, Zhang Y, Reichheld J-P, Fernie AR, Hagemann M, Timm S. **2019b**. Redox-regulation of photorespiration through mitochondrial thioredoxin o1. *Plant Physiology* **181**: 442–457.

Robaina-Estévez S, Daloso DM, Zhang Y, Fernie AR, Nikoloski Z. **2017**. Resolving the central metabolism of Arabidopsis guard cells. *Scientific Reports* **7**: 1–13.

Rocha M, Licausi F, Araujo WL, Nunes-Nesi A, Sodek L, Fernie AR, van Dongen JT. **2010**. Glycolysis and the tricarboxylic acid cycle are linked by alanine aminotransferase during hypoxia induced by waterlogging of lotus japonicus. *Plant Physiology* **152**: 1501–1513.

Schwender J, Shachar-Hill Y, Ohlrogge JB. **2006**. Mitochondrial metabolism in developing embryos of *Brassica napus*. *Journal of Biological Chemistry* **281**: 34040–34047.

Shameer S, Ratcliffe RG, Sweetlove LJ. **2019**. Leaf energy balance requires mitochondrial respiration and export of chloroplast NADPH in the light. *Plant Physiology* **180**: 1947–1961.

Shi J, Yi K, Liu Y, Xie L, Zhou Z, Chen Y, Hu Z, Zheng T, Liu R, Chen Y, *et al.* 2015. Phosphoenolpyruvate carboxylase in arabidopsis leaves plays a crucial role in carbon and nitrogen metabolism. *Plant Physiology* **167**: 671–681.

Sienkiewicz-Porzucek A, Sulpice R, Osorio S, Krahnert I, Leisse A, Urbanczyk-Wochniak E, Hodges M, Fernie AR, Nunes-Nesi A. **2010**. Mild reductions in mitochondrial NAD-dependent isocitrate dehydrogenase activity result in altered nitrate assimilation and pigmentation but do not impact growth. *Molecular Plant* **3**: 156–173.

Silva WB, Daloso DM, Fernie AR, Nunes-Nesi A, Araújo WL. **2016**. Can stable isotope mass spectrometry replace radiolabelled approaches in metabolic studies? *Plant Science* **249**: 59–69.

Steinhauser D, Fernie AR, Araújo WL. **2012**. Unusual cyanobacterial TCA cycles: Not broken just different. *Trends in Plant Science* **17**: 503–509.

Souza LP de, Fernie AR, Tohge T. **2018a**. Carbon atomic survey for identification of selected metabolic fluxes. *Plant Metabolomics*. Humana Press:59–67.

Souza PVL, Lima-Melo Y, Carvalho FE, Reichheld J-P, Fernie AR, Silveira JAG, Daloso DM. **2018b**. Function and compensatory mechanisms among the components of the chloroplastic redox network. *Critical Reviews in Plant Sciences* **2689**: 1–28.

Sulpice R, Sienkiewicz-Porzucek A, Osorio S, Krahnert I, Stitt M, Fernie AR, Nunes-Nesi A. **2010**. Mild reductions in cytosolic NADP-dependent isocitrate dehydrogenase activity result in lower amino acid contents and pigmentation without impacting growth.

Amino Acids **39**: 1055–1066.

Sweetlove LJ, Beard KFM, Nunes-Nesi A, Fernie AR, Ratcliffe RG. **2010**. Not just a circle: Flux modes in the plant TCA cycle. *Trends in Plant Science* **15**: 462–470.

Sweetlove LJ, Williams TCR, Cheung CYM, Ratcliffe RG. **2013**. Modelling metabolic CO_2 evolution - a fresh perspective on respiration. *Plant, Cell & Environment* **36**: 1631–1640.

Szecowka M, Heise R, Tohge T, Nunes-Nesi A, Vosloh D, Huege J, Feil R, Lunn J, Nikoloski Z, Stitt M, *et al.* 2013. Metabolic fluxes in an illuminated Arabidopsis rosette. *The Plant Cell* **25**: 694–714.

Tcherkez G, Boex-Fontvieille E, Mahé A, Hodges M. 2012. Respiratory carbon fluxes in leaves. *Current Opinion in Plant Biology* **15**: 308–314.

Tcherkez G, Cornic G, Bligny R, Gout E, Ghashghaie J. **2005**. In vivo respiratory metabolism of illuminated leaves. *Plant Physiology* **138**: 1596–1606.

Tcherkez G, Mahe A, Gauthier P, Mauve C, Gout E, Bligny R, Cornic G, Hodges M. **2009**. In folio respiratory fluxomics revealed by ^{13}C Isotopic labeling and H/D isotope effects highlight the noncyclic nature of the tricarboxylic acid 'cycle' in illuminated leaves. *Plant Physiology* **151**: 620–630.

Thelen JJ, Miernyk JA, Randall DD. 2000. Pyruvate dehydrogenase kinase from Arabidopsis thaliana: a protein histidine kinase that phosphorylates serine residues. *Biochemical Journal* **349**: 195-201.

Timm S, Wittmiß M, Gamlien S, Ewald R, Florian A, Frank M, Wirtz M, Hell R, Fernie AR, Bauwe, H. 2015. Mitochondrial dihydrolipoyl dehydrogenase activity shapes photosynthesis and photorespiration of Arabidopsis thaliana. *The Plant Cell* **27**: 1968-1984.

Tovar-Méndez A, Miernyk JA, Randall DD. **2003**. Regulation of pyruvate dehydrogenase complex activity in plant cells. *European Journal of Biochemistry* **270**: 1043–1049.

Vani T, Raghavendra AS. **1994**. High mitochondrial activity but lncomplete engagement of the cyanide-resistant alternative pathway in guard cell protoplasts of pea. *Plant physiology* **105**: 1263–1268.

Wang SW, Li Y, Zhang XL, Yang HQ, Han XF, Liu ZH, Shang ZL, Asano T, Yoshioka Y, Zhang CG, *et al.* 2014a. Lacking chloroplasts in guard cells of crumpled leaf attenuates

stomatal opening: Both guard cell chloroplasts and mesophyll contribute to guard cell ATP levels. *Plant, Cell & Environment* **37**: 2201–2210.

Wang Y, Noguchi K, Ono N, Inoue S, Terashima I, Kinoshita T. **2014b**. Overexpression of plasma membrane H+-ATPase in guard cells promotes light-induced stomatal opening and enhances plant growth. *Proceedings of the National Academy of Sciences of the United States of America* **111**: 533–8.

Williams TCR, Miguet L, Masakapalli SK, Kruger NJ, Sweetlove LJ, Ratcliffe RG. **2008**. Metabolic network fluxes in heterotrophic Arabidopsis cells: stability of the flux distribution under different oxygenation conditions. *Plant Physiology* **148**: 704–718.

Willmer C, Fricker M. **1996**. *Stomata.* London: Chapman & Hall.

Xu Z, Ma J, Qu C, Hu Y, Hao B, Sun Y, Liu Z, Yang H, Wang H, Li Y, Liu G. 2017. Identification and expression analyses of the alanine aminotransferase (AlaAT) gene family in poplar seedlings. *Scientific reports* **7*:*** 1-13.

Yoshida K, Hisabori T. **2014**. Mitochondrial isocitrate dehydrogenase is inactivated upon oxidation and reactivated by thioredoxin-dependent reduction in Arabidopsis. *Frontiers in Environmental Science* **2**: 1–7.

Zamboni N, Fendt S-M, Rühl M, Sauer U. **2009**. ^{13}C-based metabolic flux analysis. *Nature Protocols* **4**: 878–892.

Zhang Y, Beard KFM, Swart C, Bergmann S, Krahnert I, Nikoloski Z, Graf A, George Ratcliffe R, Sweetlove LJ, Fernie AR, *et al.* 2017. Protein-protein interactions and metabolite channelling in the plant tricarboxylic acid cycle. *Nature Communications* **8**: 1–11.

Zhao Z, Assmann SM. **2011**. The glycolytic enzyme, phosphoglycerate mutase, has critical roles in stomatal movement, vegetative growth, and pollen production in Arabidopsis thaliana. *Journal of Experimental Botany* **62**: 5179–5189.

Figures

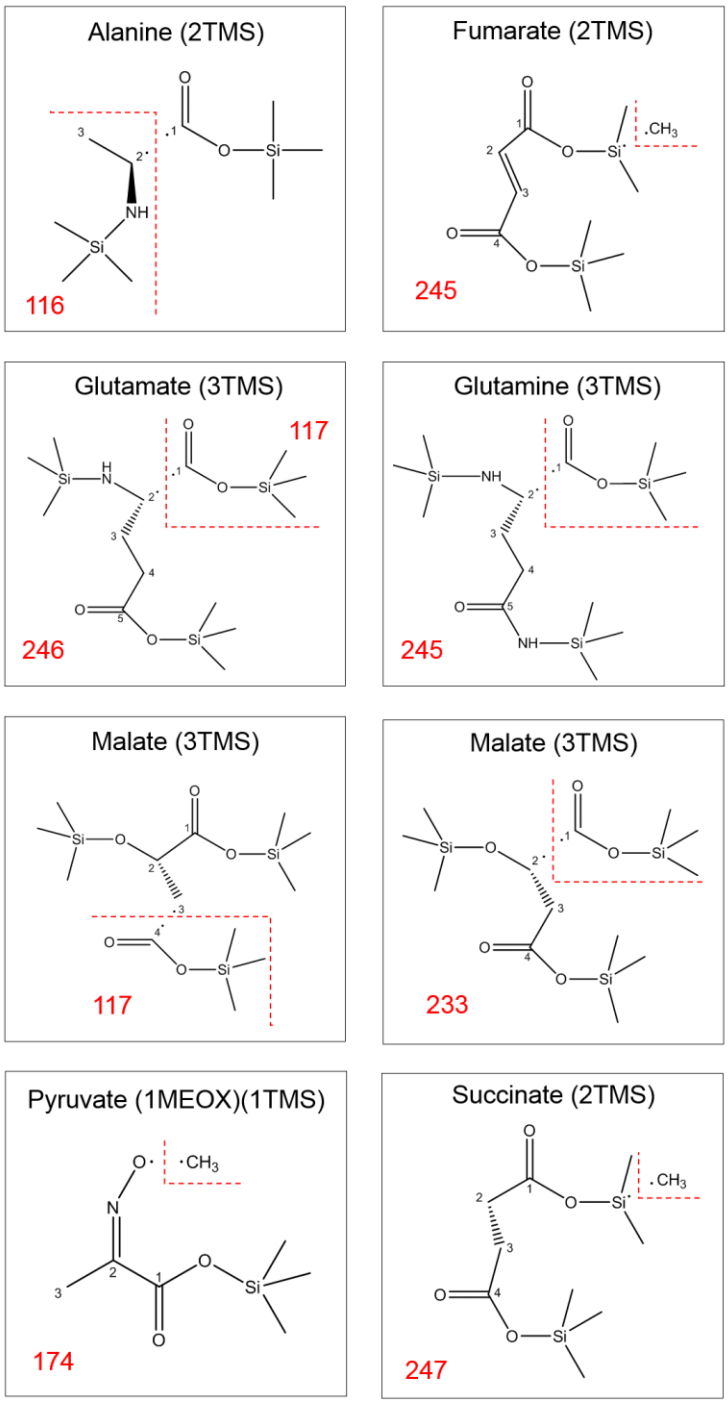

Figure 1. Estimated EI-fragmentation map of TMS-derivatized metabolites of, or related to, the TCA cycle.

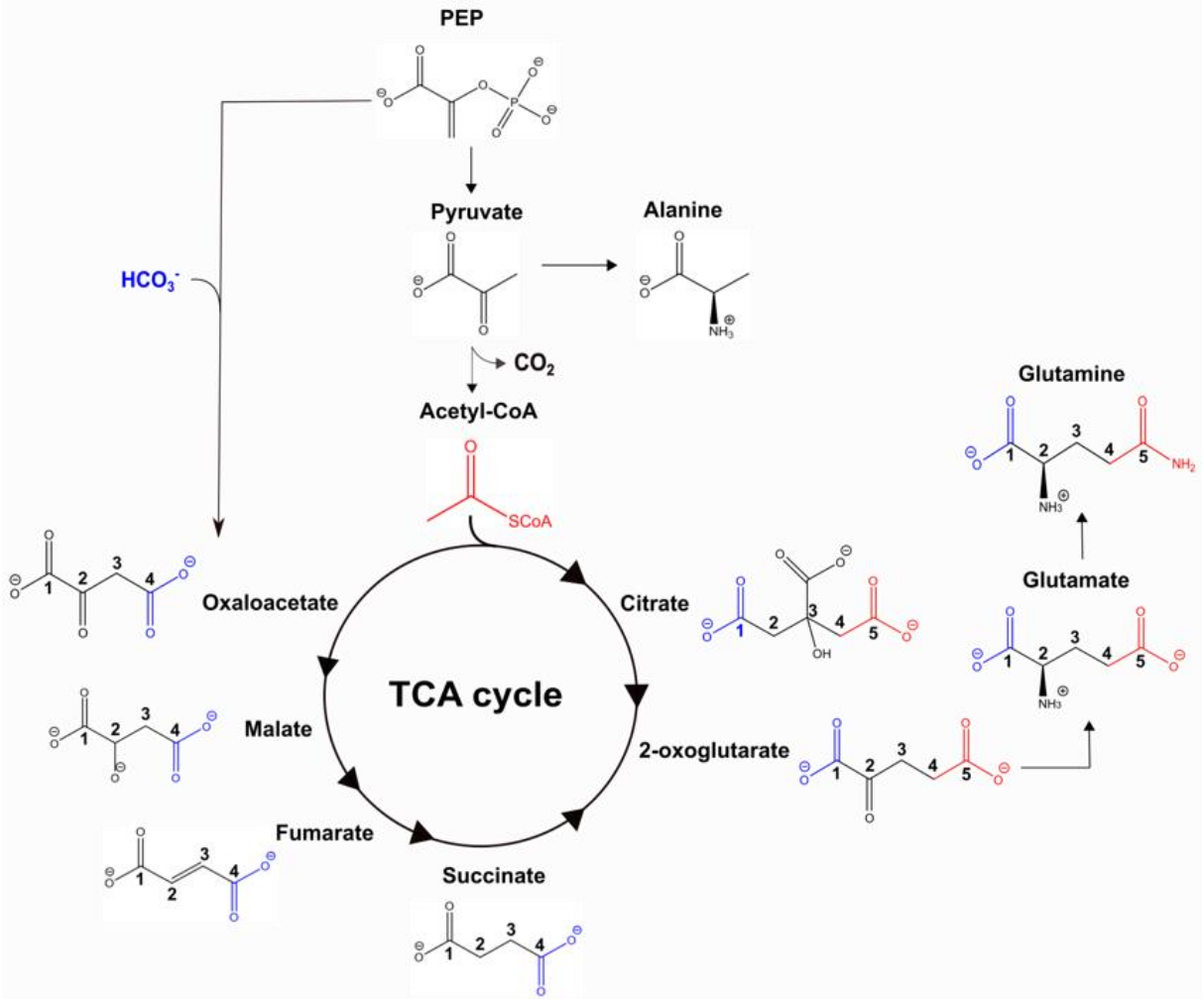

Figure 2. Simplified TCA cycle with carbon labelling from PEPc, glycolysis and TCA cycle. Malate sinthesis through oxaloacetate and the carbon 4 correspondent to PEPc HCO_3 fixation (highlighted in blue) and glutamine synthesis with carbon 1 from PEPc activity (highlighted in blue), carbon 5 from AcCoA (highlighted in red).

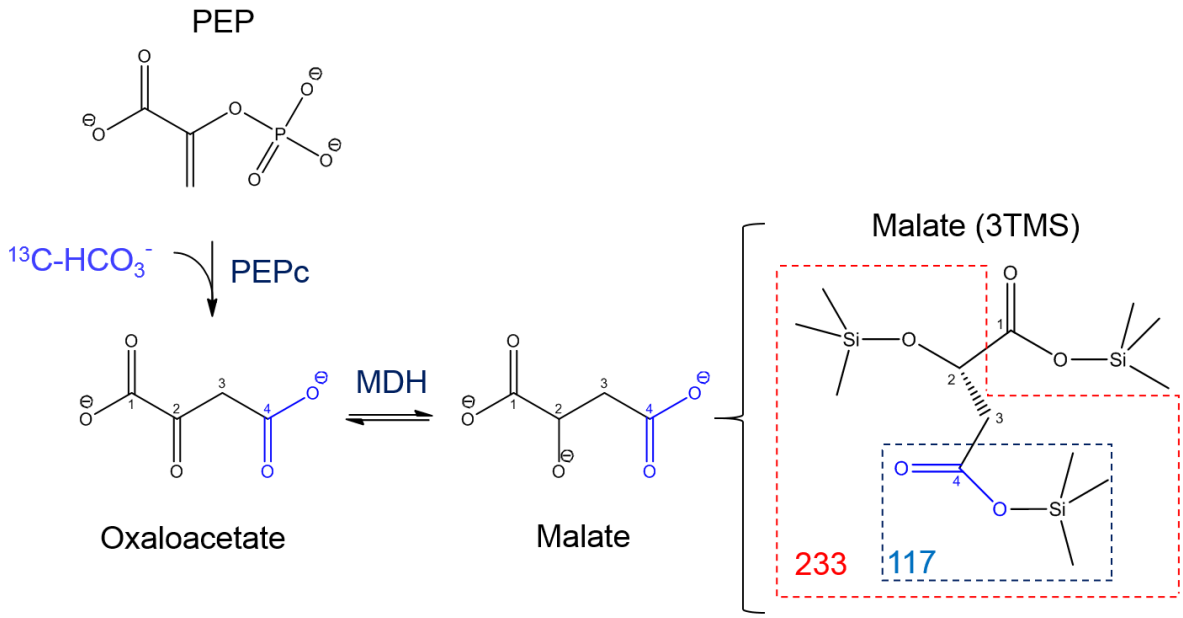

Figure 3. Carbon fixation via PEPc (highlighted in blue) through oxaloacetate synthesys and interconversion into Mal by MDH, and Mal EI-fragmentation of TMS-derivatized Mal. Fragments of Mal *m/z* 233 corresponds to carbons 2, 3 and 4, whilst *m/z* 117 to carbon 4.

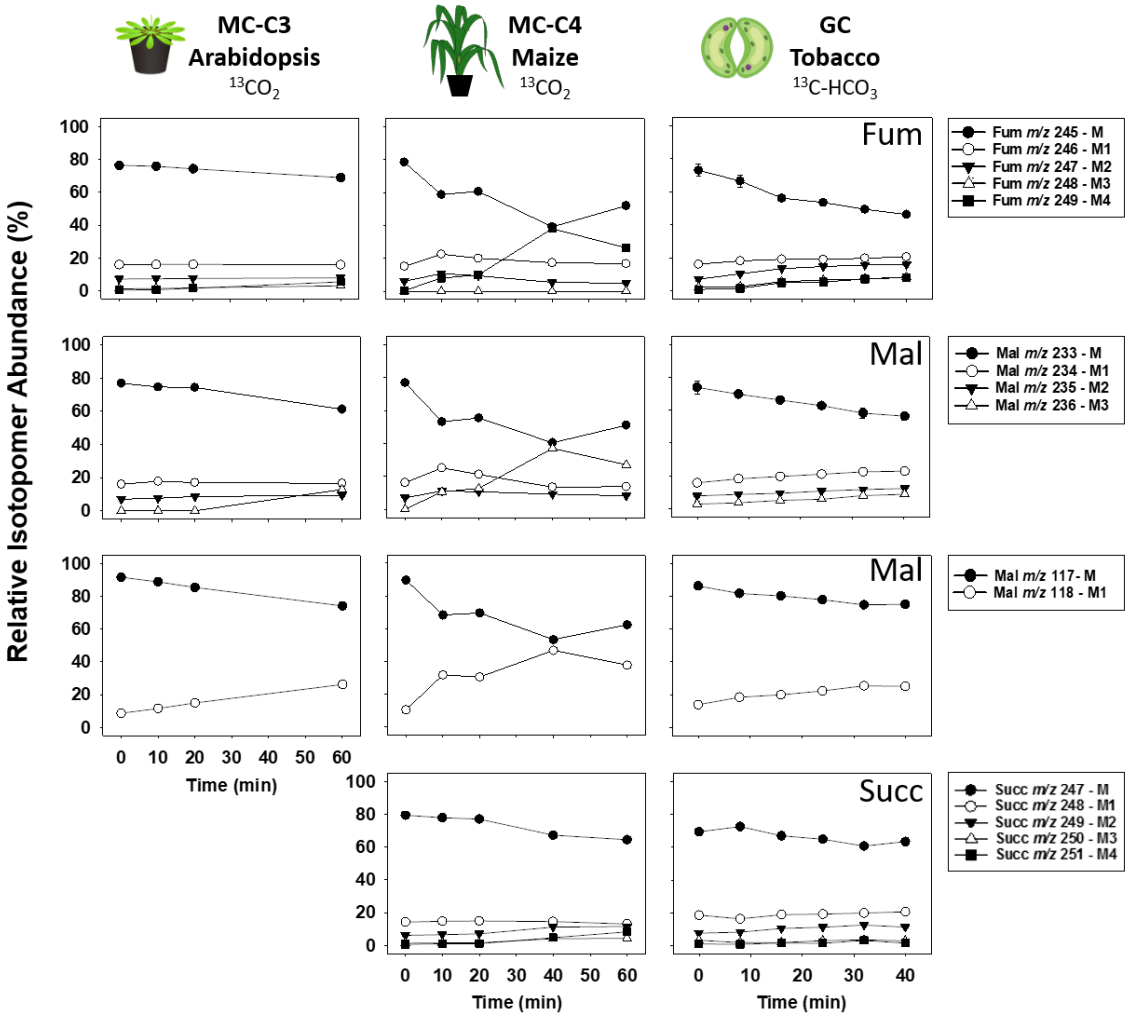

Figure 4. Relative isotopomer abundance (%) shifts of TCA cycle metabolites (Fum, Mal and Succ) in Arabidopsis (MC-C3) and maize leaves (MC-C4) during 60 minutes of incubation in $^{13}CO_2$ and in tobacco GCs during 40 minutes of incubation in $^{13}C\text{-}HCO_3$. Values are presented as mean for MC-C3 and GCs (n=3; n=4). MC-C4 has no biological replicate.

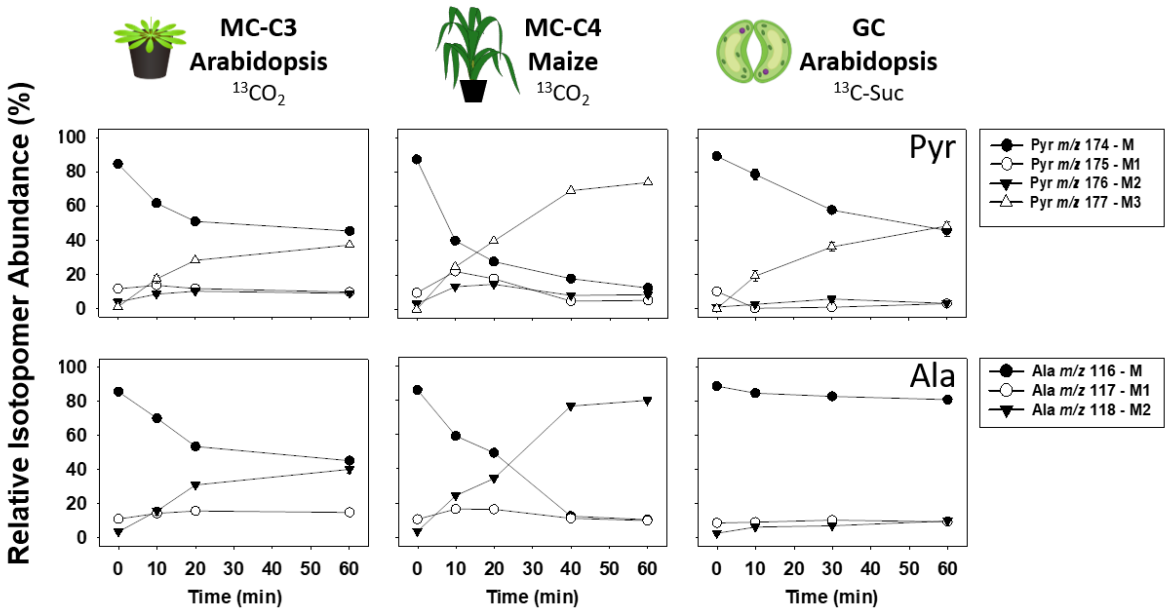

Figure 5. Relative isotopomer abundance (%) shifts of Pyr and Ala of Arabidopsis (MC-C3) and maize leaves (MC-C4) under $^{13}CO_2$ and tobacco GC under ^{13}C-Suc during 60 minutes of incubation. Values are presented as mean for MC-C3 and GCs (n=3; n=4). MC-C4 has no biological replicate.

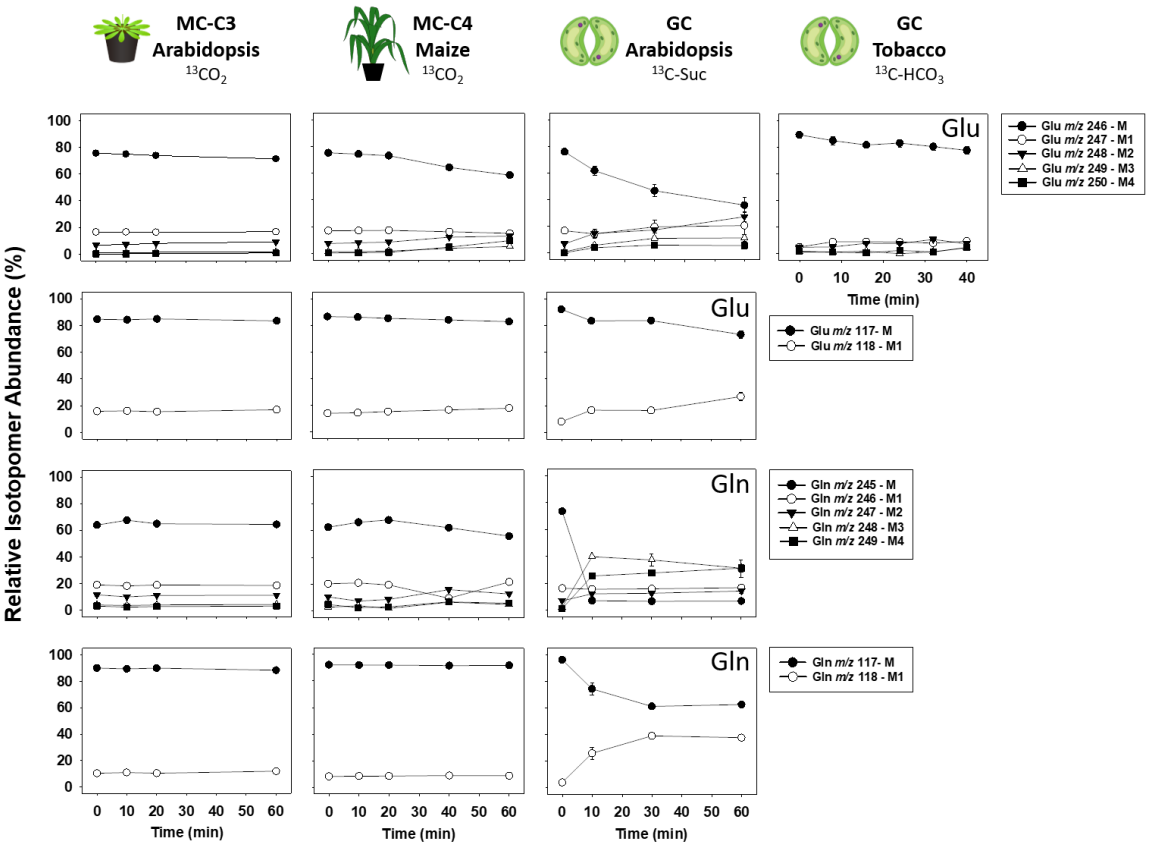

Figure 6. Relative isotopomer abundance (%) of Glu and Gln in Arabidopsis (MC-C3) and maize leaves (MC-C4) under $^{13}CO_2$ and in Arabidopsis and tobacco GCs under ^{13}C-Suc during 60 minutes of incubation or ^{13}C-HCO_3 during 40 minutes of incubation. Values are presented as mean ± SE for MC-C3 and GCs (n=3; n=4). MC-C4 has no biological replicates.

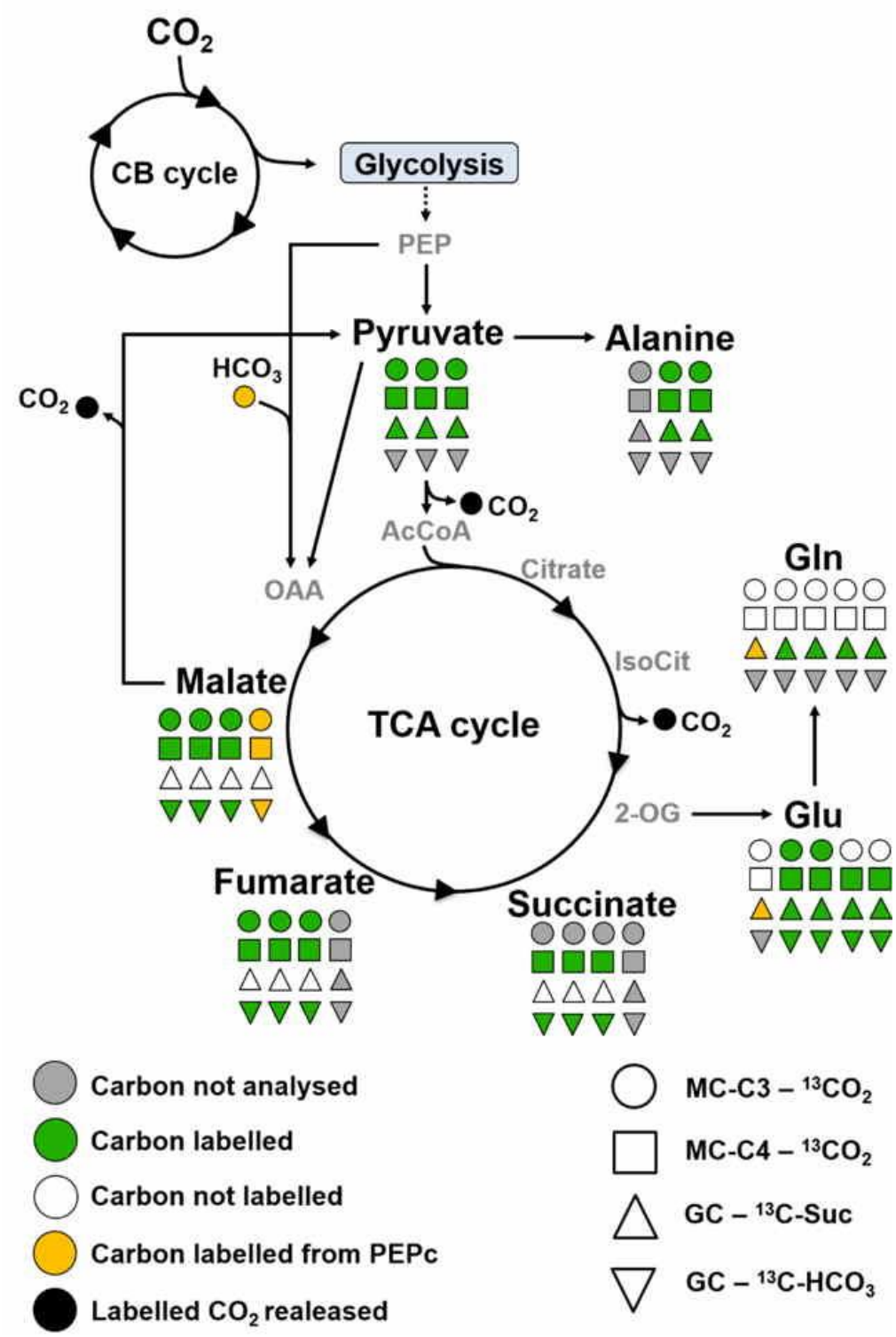

Figure 7. Schematic representation of isotope redistribution in Arabidopsis (MC-C3) and maize leaves (MC-C4) and in Arabidopsis and tobacco GCs during ^{13}C-isotope labelling kinetic experiments.

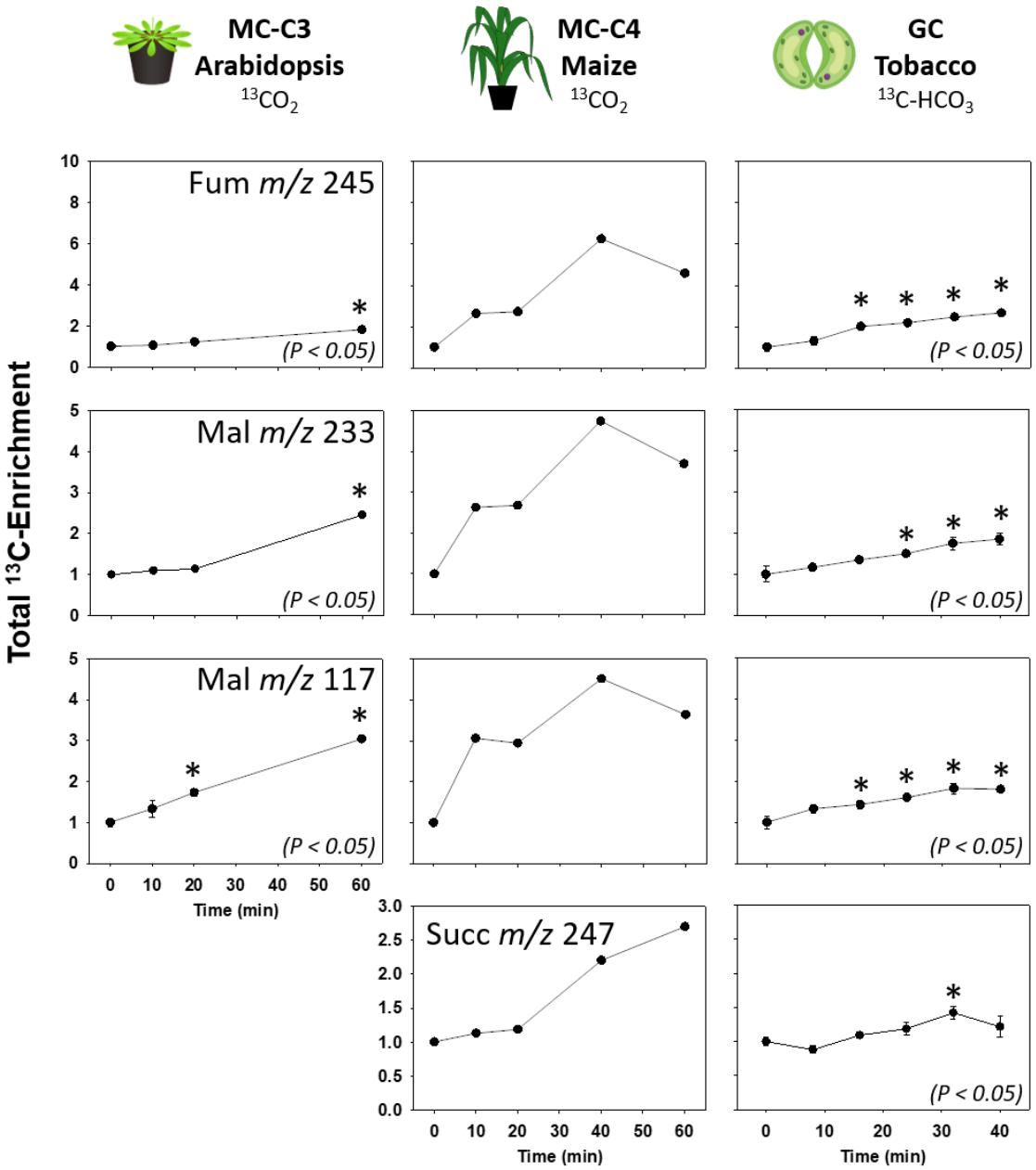

Figure 8. Total enrichment of TCA cycle metabolites normalized by time 0 (Fum, Mal and Succ) in Arabidopsis (MC-C3) and maize leaves (MC-C4) during 60 minutes of incubation in $^{13}CO_2$ and in tobacco GCs during 40 minutes of incubation in $^{13}C\text{-}HCO_3$. Values are presented as mean ± SE for MC-C3 and GCs (n=3; n=4). MC-C4 has no biological replicate. Asterisks indicate values significantly different from time 0 by the Dunnet's test (*P< 0.05).

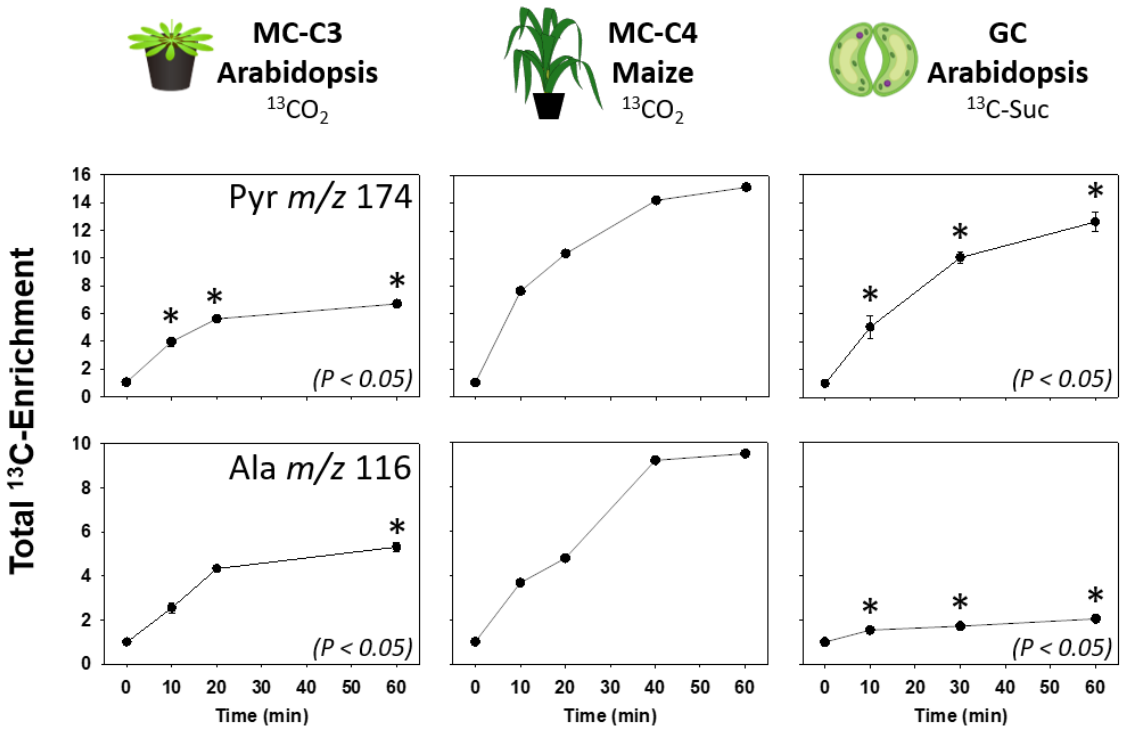

Figure 9. Total enrichment normalized by time 0 of Pyr and Ala in Arabidopsis (MC-C3) and maize leaves (MC-C4) during 60 minutes of incubation in $^{13}CO_2$ and in Arabidopsis GCs during 40 minutes of incubation in ^{13}C-HCO_3. Values are presented as mean ± SE for MC-C3 and GCs (n=3; n=4). MC-C4 has no biological replicate. Asterisks indicate values significantly different from time 0 by the Dunnet's test (*P< 0.05).

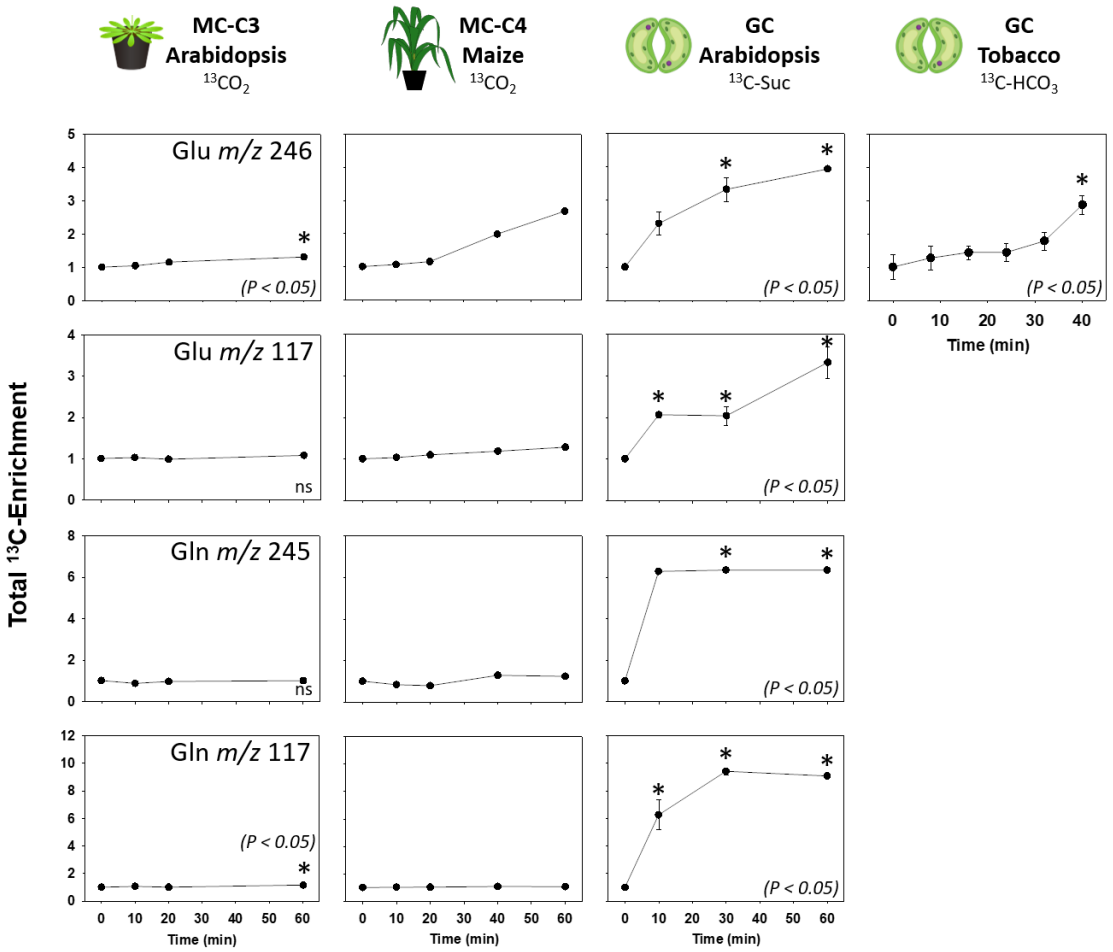

Figure 10. Normalized total ^{13}C-enrichment of Glu and Gln in Arabidopsis (MC-C3) and maize leaves (MC-C4) during 60 minutes of incubation in $^{13}CO_2$ and Arabidopsis and tobacco GCs under incubation of ^{13}C-Suc and $^{13}C-HCO_3$ during 60 and 40 minutes, respectively. Values are presented as mean ± SE for MC-C3 and GCs (n=3; n=4). MC-C4 has no biological replicates. Asterisks indicate values significantly different from time 0 by the Dunnet's test (*P< 0.05).

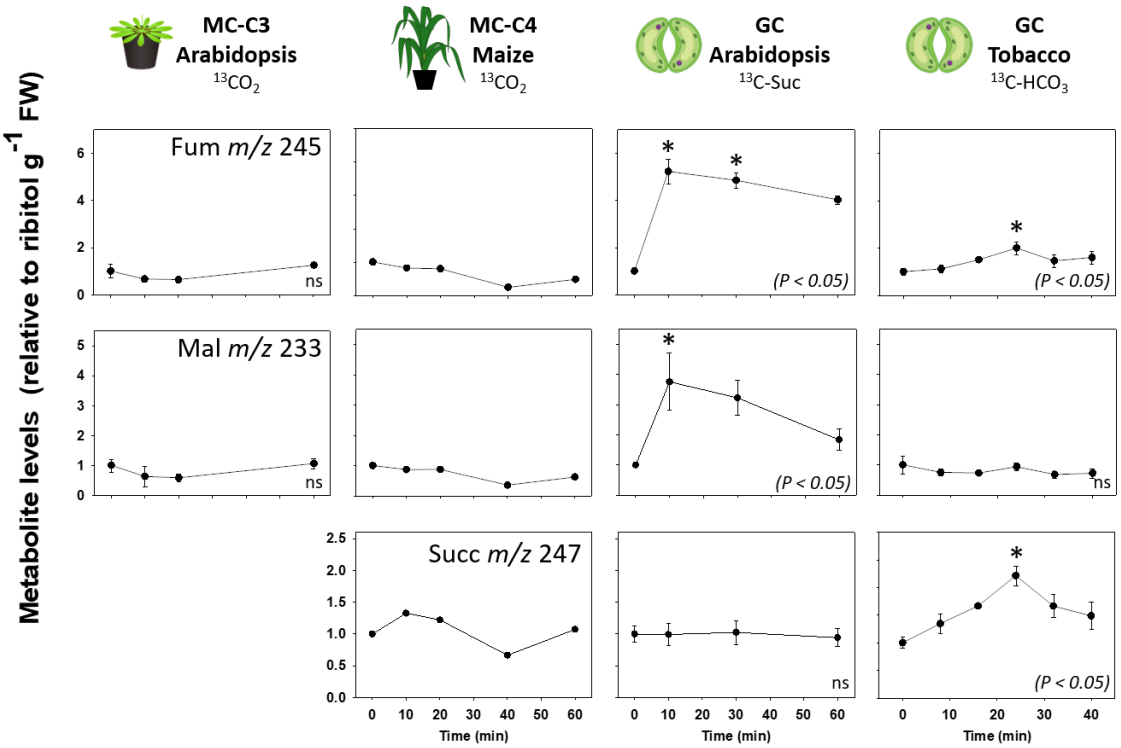

Figure 11. Normalized metabolite levels of TCA cycle metabolites (Fum, Mal and Succ) of Arabidopsis (MC-C3) and maize leaves (MC-C4) during 60 minutes of incubation in $^{13}CO_2$ and of Arabidopsis and tobacco GCs during 60 and 40 minutes under incubation in ^{13}C-Suc and ^{13}C-HCO_3, respectively. Values are presented as mean ± SE for MC-C3 and GCs (n=3; n=4). MC-C4 has no biological replicates. Asterisks indicate values significantly different from time 0 by the Dunnet's test (*P< 0.05).

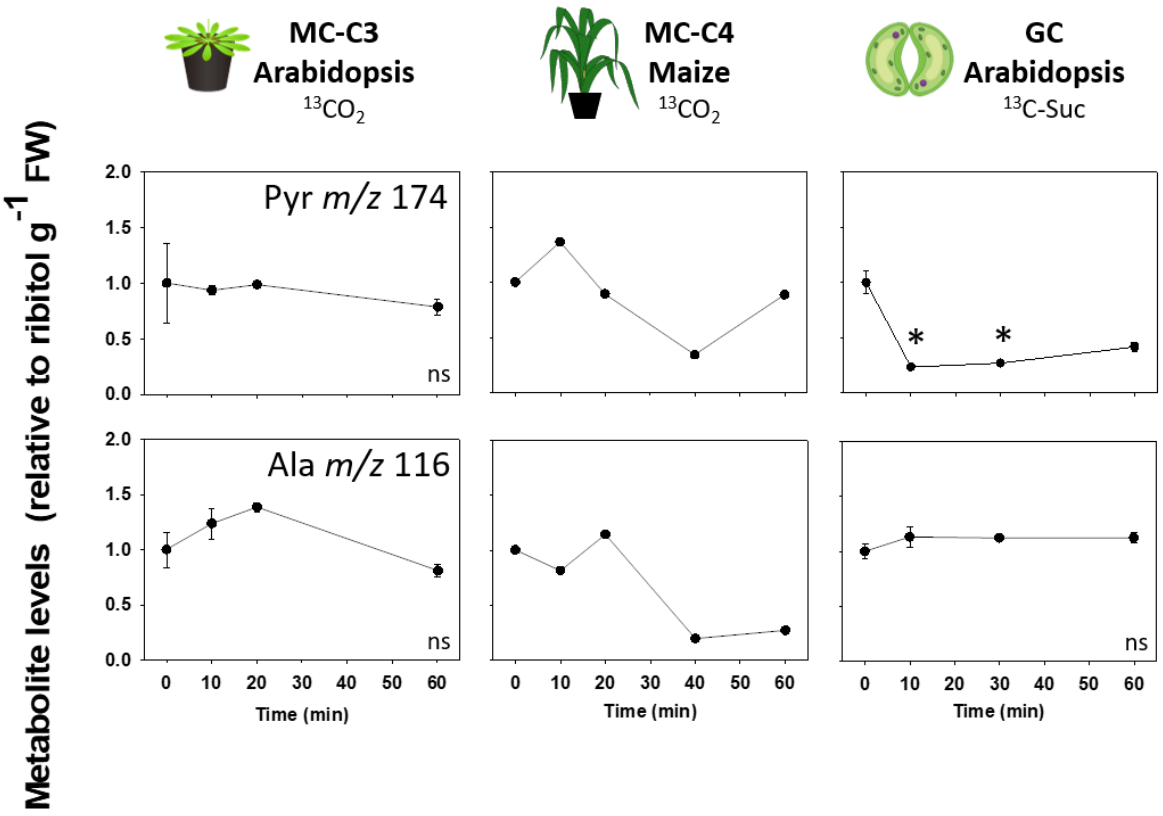

Figure 12. Normalized metabolite relative levels of Pyr and Ala of Arabidopsis (MC-C3) and maize leaves (MC-C4) during 60 minutes of incubation in $^{13}CO_2$ and Arabidopsis GCs during 60 minutes of incubation in ^{13}C-Suc. Values are presented as mean ± SE for MC-C3 and GCs (n=3; n=4). MC-C4 has no biological replicates. Asterisks indicate values significantly different from time 0 by the Dunnet's test (*P< 0.05).

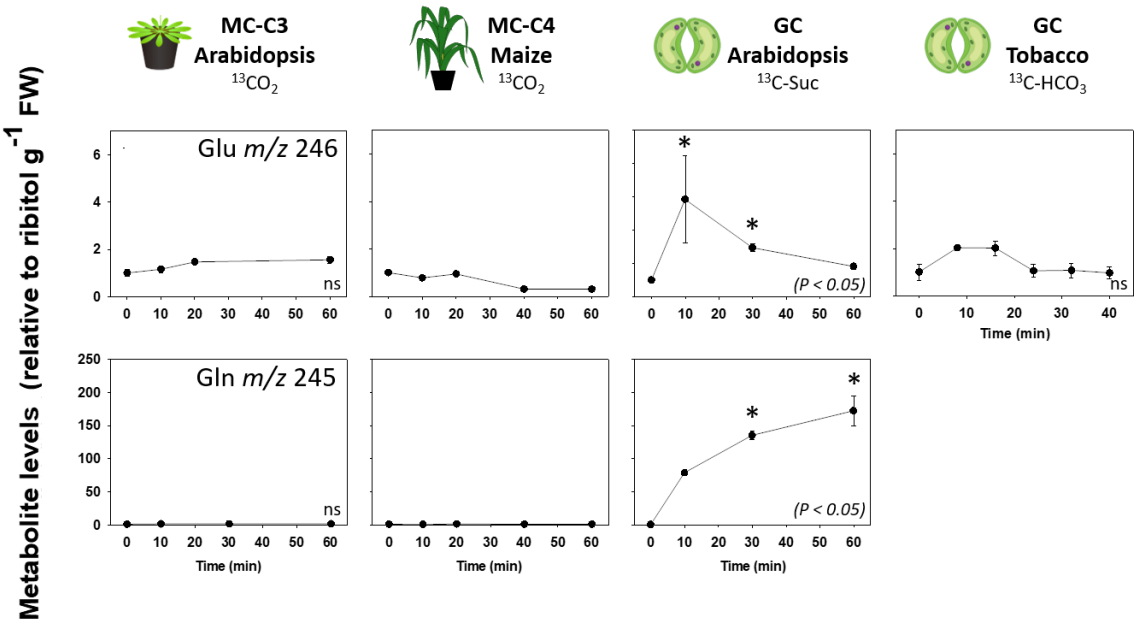

Figure 13. Normalized metabolite relative levels of Glu and Gln of Arabidopsis (MC-C3) and maize leaves (MC-C4) during 60 minutes of incubation in $^{13}CO_2$ and of Arabidopsis and tobacco GCs under ^{13}C-Suc and ^{13}C-HCO_3 during 60 and 40 minutes of incubation, respectively. Values are presented as mean ± SE for MC-C3 and GCs (n=3; n=4). MC-C4 has no biological replicates. Asterisks indicate values significantly different from time 0 by the Dunnet's test (*P< 0.05).

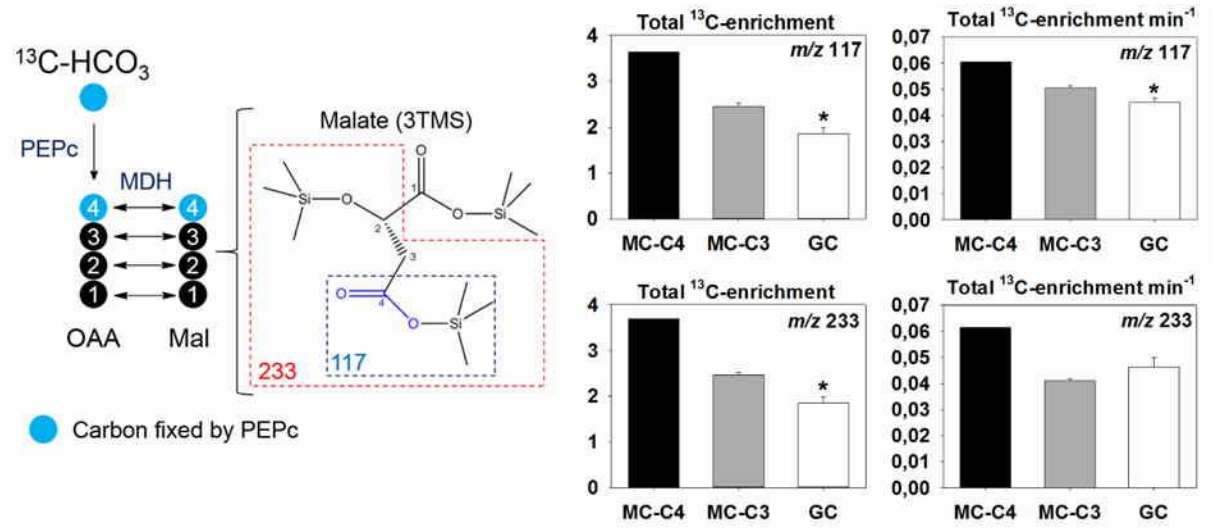

Figure 14. Schematic representation of PEPc anaplerotic fixation of HCO_3 into oxaloacetate, normalized total ^{13}C-enrichment and total ^{13}C-enrichment min^{-1} of Mal *m/z* 233 (carbons 2 – 4) and 117 (carbon 4) of maize (MC-C4) and Arabidopsis leaves (MC-C3) under $^{13}CO^2$ and tobacco GCs under ^{13}C-HCO_3. Values are presented as mean ± SE for MC-C3 and GCs (n=3; n=4). MC-C4 has no biological replicates. Asterisks indicate values significantly different from time 0 by Student's *t*-test (*P< 0.05).

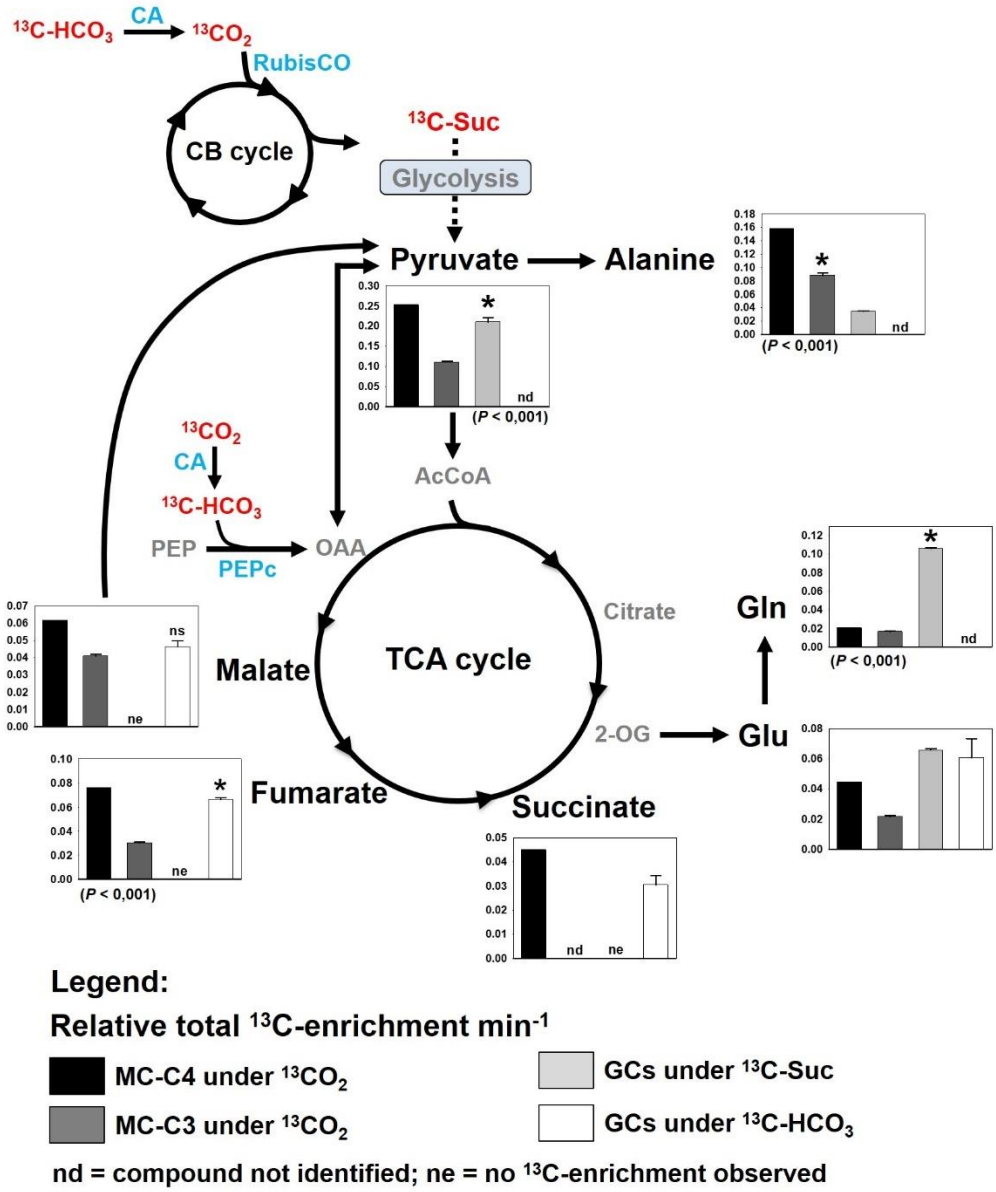

Figure 15. TCA cycle diagram with relative total ^{13}C-enrichment min^{-1} of Pyr, Ala, Glu, Gln, Fum, Mal and Succ of Arabidopsis (MC-C3) and maize leaves (MC-C4) under incubation of $^{13}CO_2$, and of Arabidopsis and tobacco GCs under $^{13}HCO_3$. Values are presented as mean ± SE for MC-C3 and GCs (n=3; n=4) MC-C4 has no biological replicates. Asterisks indicate values significantly different from time 0 by Student's *t*-test (*P< 0.05).

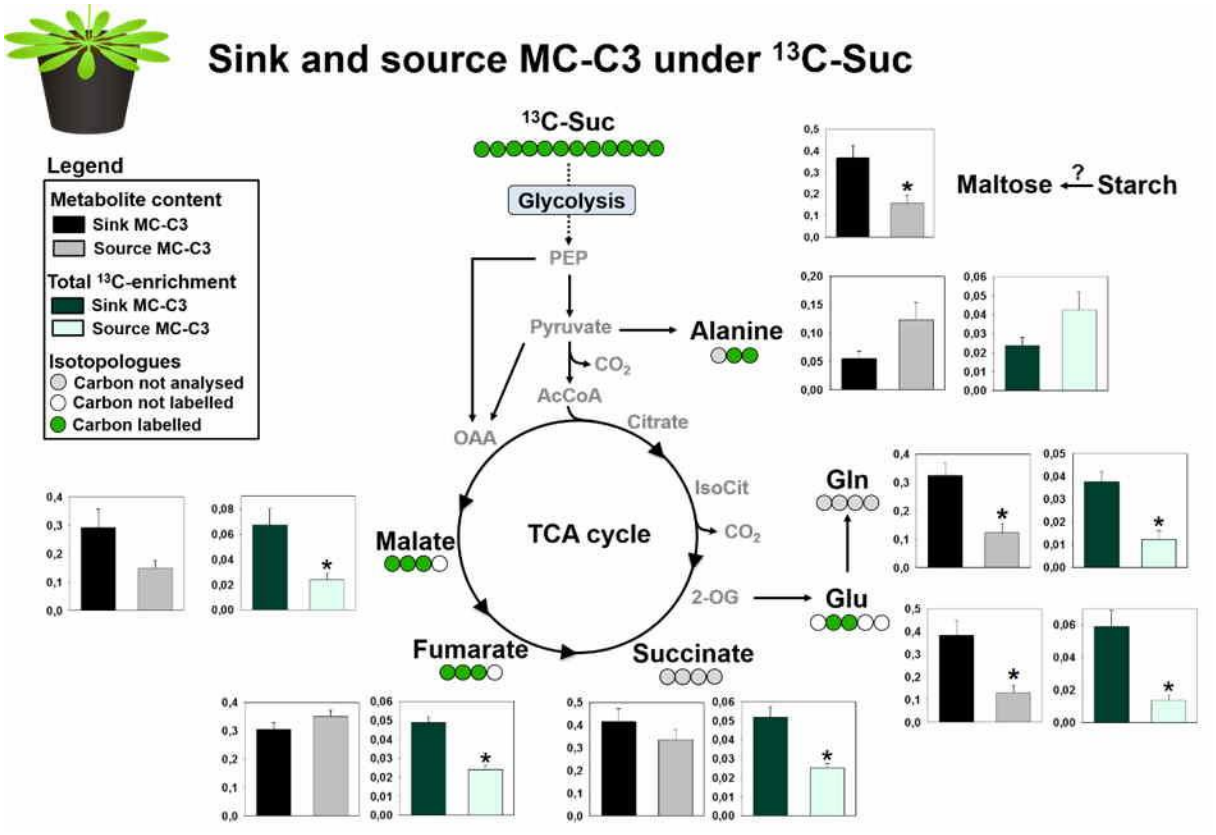

Figure 16. TCA cycle diagram with metabolite content and total ^{13}C-enrichment normalized by time 0 of Arabidopsis sink and source leaves under ^{13}C-Suc. Values are presented as mean ± SE (n=4). Asterisks indicate values significantly different by Student's *t*-test (*P< 0.05).

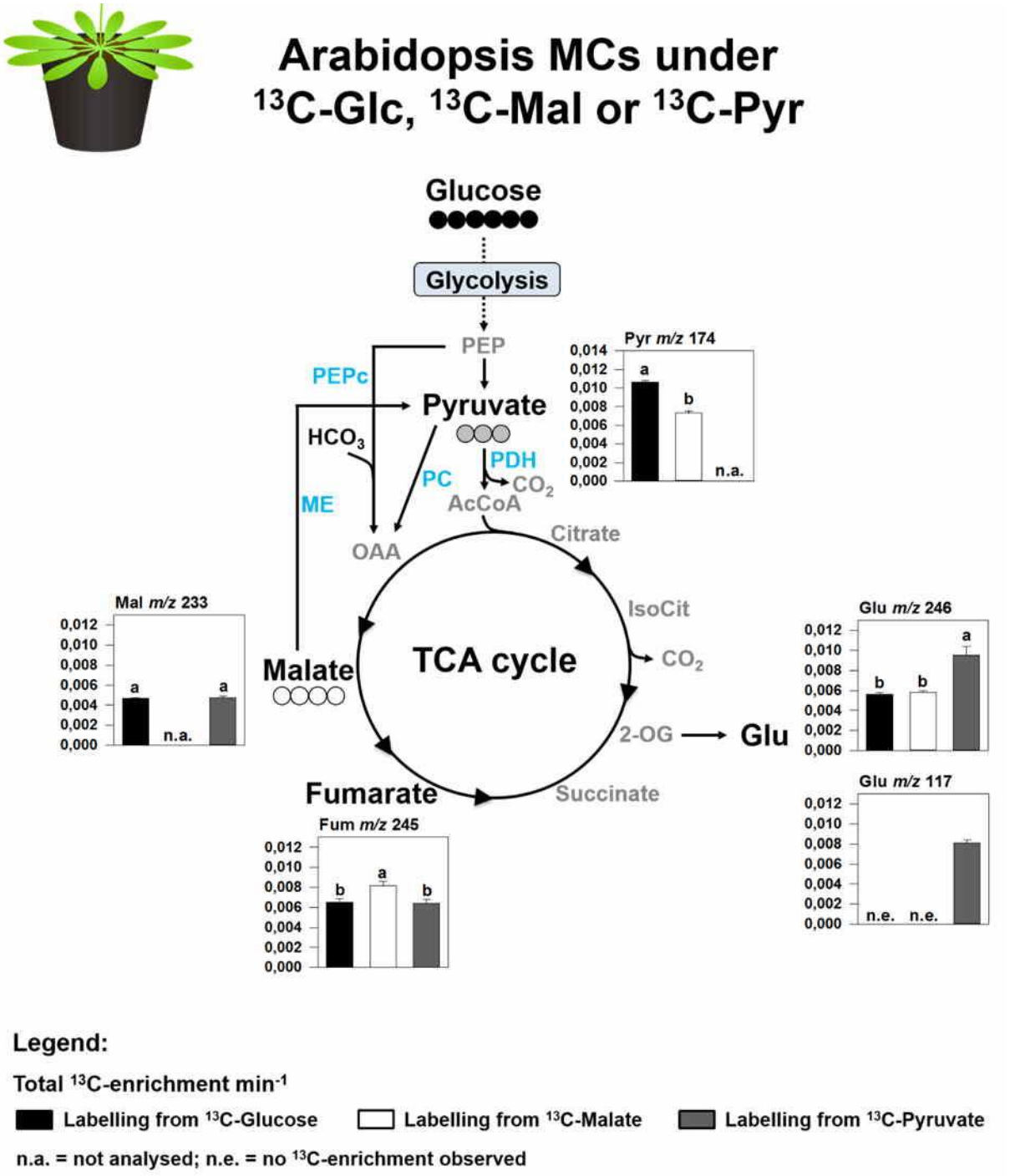

Figure 17. TCA cycle diagram with total ^{13}C-enrichment min^{-1} of Arabidopsis (WT) leaves under ^{13}C-Glucose, ^{13}C-Malate and ^{13}C-Pyruvate. Values are presented as mean ± SE (n=4). Identical letters, lower case among C labelled do not significantly differ by Tukey's test (P< 0.05).

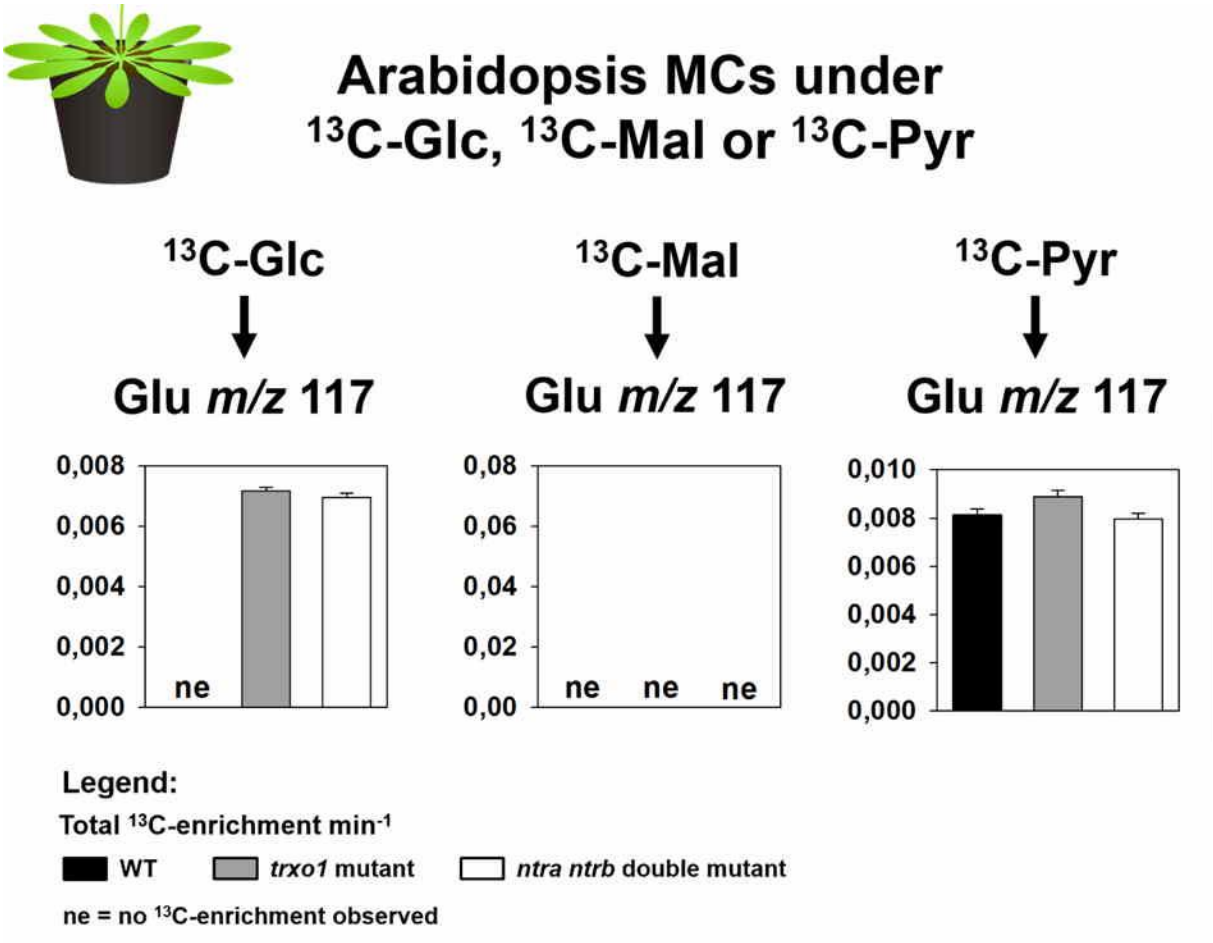

Figure 18. Total ^{13}C-enrichment min^{-1} of Glu *m/z* 117 of Arabidopsis leaves of plants lacking *trxo1*, *ntrb ntra* and wild type plants under ^{13}C-Glucose, ^{13}C-Malate and ^{13}C-Pyruvate. Values are presented as mean ± SE (n=4). Identical letters, lower case among C labelled do not significantly differ by Tukey's test ($P< 0.05$).

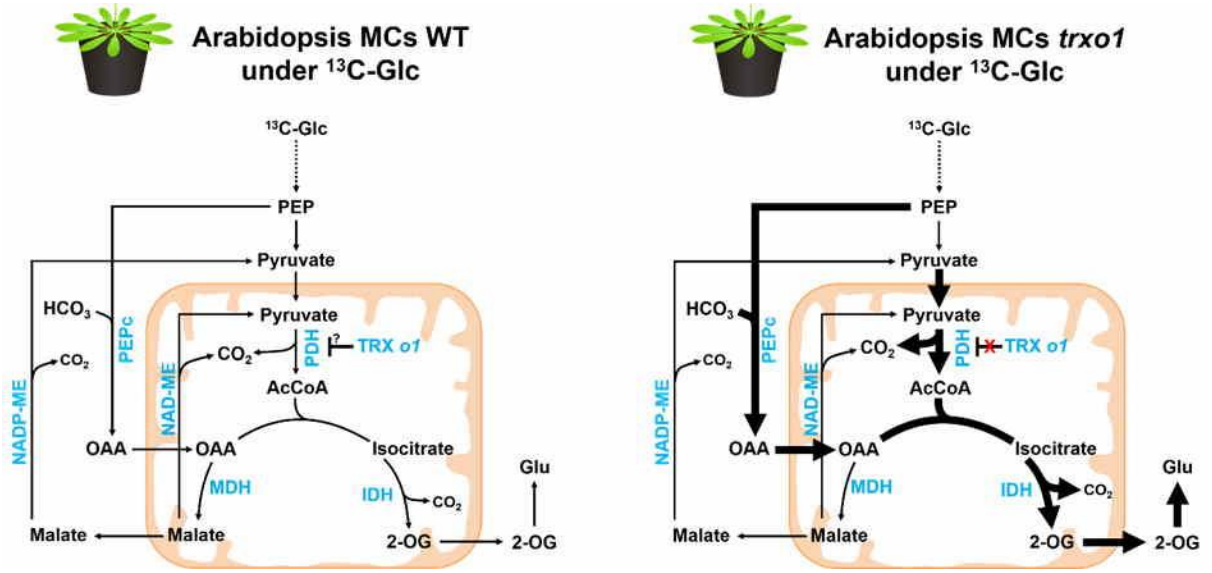

Figure 19. Schematic representation summarizing the differences of TCA cycle regulation among Arabidopsis leaves (MC-C3) of WT and *trxo1* mutant under ^{13}C-Glc.

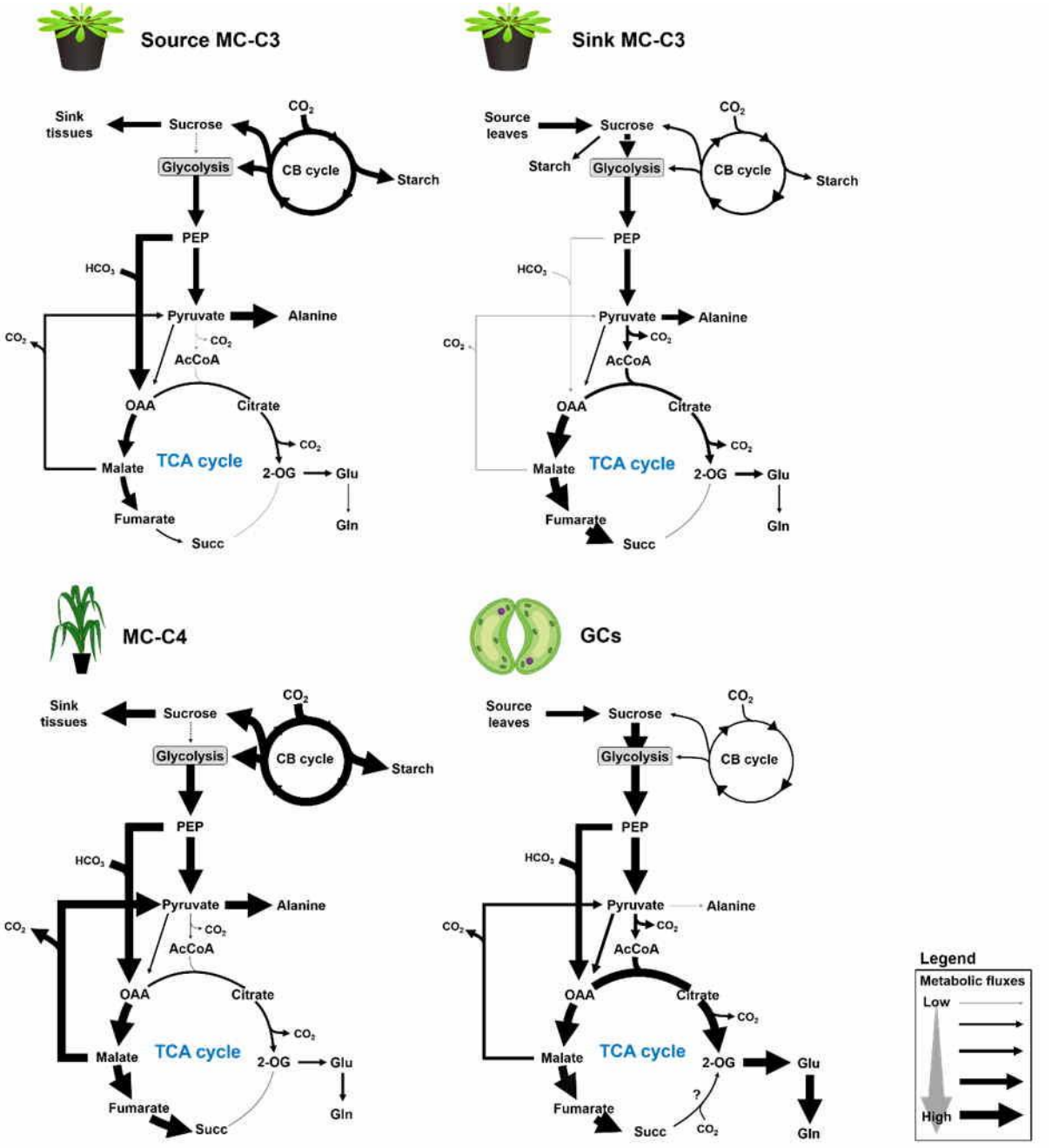

Figure 20. Metabolic network of the Calvin-Benson cycle, glycolysis, TCA cycle and associated pathways of source and sink Arabidopsis leaves (MC-C3), maize leaves (MC-C4 and GCs.

Table S1. Details of data set used in the meta-analysis. Chromatograms of primary metabolites identified by GC-EI-TOF-MS were kindly provided by the following authors.

Tissue labelled	**Species**	**^{13}C-substrate**	**Experiment condition**	**Sample harvesting (min)**	**MS platform**	**Reference**
GC	Arabidopsis	^{13}C-Suc	Dark-to-light transition	0, 10, 30 and 60	GC-EI-TOF-MS	(Medeiros *et al.*, 2018)
GC	Tobacco	^{13}C-HCO_3^-	Dark-to-light transition	0, 8, 16, 24, 32 and 40	GC-EI-TOF-MS	(Daloso *et al.*, 2015a)
Leaves	Maize	$^{13}CO_2$	Light condition	0, 10, 20,40 and 60	GC-EI-TOF-MS	(Arrivault *et al.*, 2017)
Leaves	Arabidopsis	$^{13}CO_2$	Light condition	0, 10, 20 and 60	GC-EI-TOF-MS	(Szecowka *et al.*, 2013)
Leaves	Arabidopsis	^{13}C-Suc	Sink and Source leaves under light condition	240	GC-EI-TOF-MS	(Dethloff *et al.*, 2017)
Leaves	Arabidopsis (WT, *ntra ntrb*, *trxo1*)	^{13}C-Mal, ^{13}C-Pyr and ^{13}C-Glc	Light condition	240	GC-EI-TOF-MS	(Daloso et al., 2015b)